



Published in final edited form as:

*Microsc Microanal.* 2018 August ; 24(4): 406–419. doi:10.1017/S1431927618012382.

## Biological Applications at the Cutting Edge of Cryo-Electron Microscopy

Rebecca S. Dillard<sup>1</sup>, Cheri M. Hampton<sup>1,§</sup>, Joshua D. Strauss<sup>1</sup>, Zunlong Ke<sup>1,2</sup>, Deanna Altomara<sup>1</sup>, Ricardo C. Guerrero Ferreira<sup>1,†</sup>, Gabriella Kiss<sup>1,‡</sup>, and Elizabeth R. Wright

<sup>1</sup>Division of Pediatric Infectious Diseases, Emory University School of Medicine, Children's Healthcare of Atlanta, Atlanta, GA 30322, USA

<sup>2</sup>School of Biological Sciences, Georgia Institute of Technology, Atlanta, GA 30332, USA

<sup>3</sup>Robert P. Apkarian Integrated Electron Microscopy Core, Emory University, Atlanta, GA 30322, USA

### Abstract

Cryo-electron microscopy (cryo-EM) is a powerful tool for macromolecular to near-atomic resolution structure determination in the biological sciences. The specimen is maintained in a near-native environment within a thin film of vitreous ice and imaged in a transmission electron microscope (TEM). The images can then be processed by a number of computational methods to produce three-dimensional information. Recent advances in sample preparation, imaging, and data processing have led to tremendous growth in the field of cryo-EM by providing higher resolution structures and the ability to investigate macromolecules within the context of the cell. Here, we review developments in sample preparation methods and substrates, detectors, phase plates, and cryo-correlative light and electron microscopy (cryo-CLEM) that have contributed to this expansion. We also have included specific biological applications.

### Keywords

Cryo-electron microscopy (cryo-EM); cryo-electron tomography (cryo-ET); cryo-correlative light and electron microscopy (cryo-CLEM); transmission electron microscopy (TEM); vitrification; phase plates; direct electron detectors

### Introduction

Cryo-electron microscopy (cryo-EM) technologies were pioneered in order to retain specimen hydration and reduce electron-beam damage to the specimen during direct imaging and electron diffraction in the transmission electron microscope (TEM) (Taylor &

<sup>#</sup>To whom correspondence should be addressed: Elizabeth R. Wright, Emory University School of Medicine, Department of Pediatrics, Division of Pediatric Infectious Diseases, 2015 Uppergate Drive NE, Atlanta, GA 30322, USA, Tel. (+1) 404-727-4665, Fax. (+1) 404-727-9223, erwright@emory.edu.

<sup>§</sup>Current address: Materials and Manufacturing Directorate, Air Force Research Laboratory, Wright Patterson AFB, Ohio 45433, United States

<sup>†</sup>Current address: Center for Cellular Imaging and NanoAnalytics (C-CINA), Biozentrum, University of Basel, Mattenstrasse 26, 4058 Basel, Switzerland

<sup>‡</sup>Current address: Thermo Fisher Scientific, 5350 NE Dawson Creek Drive, Hillsboro, Oregon 97124, United States

Glaeser, 1974). Initial work focused on catalase crystals preserved in a thin film of vitreous ice (Taylor & Glaeser, 1974). Subsequently, suspensions of viruses and other samples were vitrified and imaged, functionally extending cryo-EM to structural investigations of broad ranges of targets (Dubochet, et al., 1983; Lepault, et al., 1983; McDowell, et al., 1983; Adrian, et al., 1984). Most aqueous samples are prepared for cryo-EM or cryo-electron tomography (cryo-ET) by first applying a small aliquot of a suspension to an electron microscope (EM) grid, blotting the grid to near dryness, and then rapidly plunge-freezing it in liquid ethane or liquid propane cooled to cryogenic temperatures. This method effectively preserves the biological sample in a thin layer of vitreous, non-crystalline ice in a near native state (Lepault, et al., 1983; Dubochet, et al., 1988). Continued developments to specimen preservation equipment and methods by research groups and EM manufacturers have improved the quality and reproducibility of the cryo-EM grids prepared.

The cryo-preserved specimens are then loaded into grid-holders, e.g. cryo-holders, which maintain the specimen at close to liquid nitrogen temperatures in order to minimize the devitrification or warming of the specimen. There have been many improvements made to these holders since their introduction in the late 1970s. Many of the cryo-holders available may be used in standard side-entry microscopes. In order to preserve specimen integrity and to facilitate high-throughput data collection, EM companies began to design and produce instruments with 'multi-specimen' cartridge-style systems in which three to twelve individual specimens can be loaded into the column of the microscope. Simultaneously, improvements to overall microscope stability, the use of field emission electron sources, computer control, and the automation of standard functions enabled the beginning of the 'resolution revolution in cryo-EM' (Kuhlbrandt, 2014), by facilitating the acquisition of high quality EM data both on film and CCD cameras via automated routines (Hewat & Neumann, 2002; Stagg, et al., 2006).

Samples prepared for single particle analysis (SPA) cryo-EM are typically purified homogeneous proteins, macromolecules, or viruses. Ideally, the sample is vitrified with particles in random orientations within a uniform layer of ice. After imaging, the particles are identified, aligned and classified, and reconstructed to produce a three-dimensional (3D) map (Cheng, et al., 2015). Heterogeneous samples, such as pleomorphic viruses, bacteria, or mammalian cells are more readily studied using cryo-ET, in which a collection of images of a vitrified single feature on the grid is acquired at various tilts, producing a tilt series. The images of the tilt series are then computationally back-projected to generate a 3D reconstruction, or tomogram, of the sample (Oikonomou & Jensen, 2017). Homogenous components within the tomogram may be extracted and further analyzed using sub-tomogram averaging (Wan & Briggs, 2016).

Recent advances in sample preparation, imaging, and data processing have led to a dramatic expansion of cryo-EM in structural biology (Cheng, et al., 2015; Nogales, 2015). The workflow for structure determination by cryo-EM is outlined in Figure 1. Sample optimization is achieved by one of several freezing steps. Vitrification of a thin film sample for SPA cryo-EM or cryo-ET is accomplished by plunge freezing. Larger sample volumes, including confluent cell layers and tissue, may be vitrified using pressure by high pressure freezing (HPF) (Dahl & Staehelin, 1989; Dubochet, 1995; Studer, et al., 2008) or self-

pressurized rapid freezing (SPRF) (Leunissen & Yi, 2009; Han, et al., 2012b; Grabenbauer, et al., 2014). The sample may be further processed after vitrification by thinning (cryo-focused ion beam milling (cryo-FIB) or cryo-sectioning) or examined by cryo-correlative light and electron microscopy (cryo-CLEM) before cryo-ET imaging and image processing. In this review, we discuss some of the recent advances at various steps of this workflow, which we have used to improve imaging of biological specimens. These include the use of new substrates and methods for sample preparation, phase plates and direct electron detectors for cryo-EM image acquisition, and the application of cryo-CLEM, which combines spatiotemporal information about the sample from fluorescence light microscopy, with structural information from cryo-EM. There have, of course, been many other developments in techniques and data processing that are described elsewhere (Bai, et al., 2015; Binshtein & Ohi, 2015; Fernandez-Leiro & Scheres, 2016; Frank, 2017; Murata & Wolf, 2018).

## Substrates and Specimen Preparation

One of the essential components of high-quality, high-resolution cryo-EM is reproducible and robust sample preparation. Cryo-EM samples are typically applied to an EM grid consisting of an amorphous holey carbon film supported by a metal mesh. The grid is then blotted to remove excess liquid and plunge-frozen in a liquid cryogen (“plunge freezing” in Figure 1), suspending the sample in a layer of vitreous ice. This process preserves the close-to-native-state structure of the hydrated specimen, but can have low throughput and be unpredictable in terms of ice thickness and particle distribution. Additionally, it has been shown that irradiation in the electron microscope leads to deformation of the amorphous carbon, causing sample movement and hence blurred images (Glaeser, et al., 2011; Brilot, et al., 2012; Russo & Passmore, 2016b). Recently, several new sample purification methods, substrates, and grid preparation systems have been developed to optimize performance during imaging, and these include affinity capture systems, gold grids, and advanced vitrification devices.

Cryo-EM single particle reconstructions are based on averaging projections of thousands of identical particles in random orientations (Guo & Jiang, 2014; Cheng, et al., 2015; Doerr, 2015; Frank, 2017). Homogeneity of the sample is therefore extremely important although such purification can be challenging. Cross-linking has been used to stabilize many heterogeneous samples for cryo-EM, such as the proteasome (Lasker, et al., 2012), spliceosome (Agafonov, et al., 2016; Wan, et al., 2016; Bertram, et al., 2017), and membrane complexes (Fiedorczuk, et al., 2016; Kosinski, et al., 2016). These studies combined cryo-EM with cross-linking mass spectrometry (CX-MS), which provides even further detail about residues that are in close proximity (Schmidt & Urlaub, 2017). An additional method for reducing heterogeneity, called GraFix, uses a weak chemical fixation during density gradient centrifugation to provide conformational stability and purify the sample, leading to a more homogenous population (Kastner, et al., 2008; Stark, 2010).

Another concern is preferred orientations of the particles on the grid. Because the sample is confined to a thin layer of vitreous ice, it can interact with both the grid support and the air-water interfaces, leading to a bias in binding and therefore nonisotropic sampling of particle

orientations (Stark, 2010). Noble *et al.* have recently shown that approximately 90% of particles on a typical cryo-EM grid prepared for single particle analysis adsorb to the air-water interfaces, potentially causing preferred particle orientations, conformational changes in the protein, or protein denaturation (Noble, et al., 2017). The use of continuous carbon support films to improve particle distribution may provide particular particle orientations, but it may also lead to even more significant orientation problems (Thompson, et al., 2016). Self-assembled monolayers (Meyerson, et al., 2014), poly-L-lysine (Chowdhury, et al., 2015), and detergents (Zhang, et al., 2011; Lyumkis, et al., 2013), have all been used to reduce preferred orientation, but tend to be sample specific (Tan, et al., 2017). The preferred orientation problem may also be addressed at the imaging level, by tilting the specimen during data collection (Tan, et al., 2017). Better sampling in Fourier space can be achieved by tilting. However, at high tilts, there is a loss of high-spatial frequency information. Tilting creates a defocus gradient that must be accounted for and corrected. In addition, the ice thickness is increased relative to the electron beam, reducing contrast in the images (Tan, et al., 2017).

Single particle cryo-EM of membrane proteins tends to be challenging because the proteins must be extracted from the membrane and solubilized in detergents, which may affect protein structure and function and reduce image contrast (Linke, 2009; Baker, et al., 2015; Efremov, et al., 2017). Amphipathic polymers called amphipols are a potential alternative to detergents. These are milder surfactants used to non-covalently bind the transmembrane portion of the protein, improving membrane protein solubility without affecting the contrast of the images. Amphipols have been used in the determination of several membrane protein structures (Flötenmeyer, et al., 2007; Althoff, et al., 2011; Cvetkov, et al., 2011; Cao, et al., 2013; Liao, et al., 2013; Lu, et al., 2014a; Wilkes, et al., 2017). Another method of preparing membrane proteins for cryo-EM is the use of lipid nanodiscs (Frauenfeld, et al., 2011; Efremov, et al., 2015; Frauenfeld, et al., 2016a; Gao, et al., 2016; Gatsogiannis, et al., 2016; Matthies, et al., 2016; Shen, et al., 2016; Jin, et al., 2017). Nanodiscs consist of scaffold proteins surrounding a small lipid bilayer in which the protein of interest is reconstituted. This maintains a near native environment for the protein and provides additional particle size, which may be helpful for particle selection, although heterogeneity of the nanodisc may be a concern (Baker, et al., 2015; Efremov, et al., 2017).

Styrene maleic acid lipid particles (SMALPs) are an alternative to nanodiscs that do not require reconstitution of membrane proteins or detergents at any stage (Hardy, et al., 2016). Styrene maleic acid (SMA) is an amphipathic co-polymer of alternating hydrophobic styrene and hydrophilic maleic acid units, which allows interaction with the membrane and provides solubility for the membrane protein. SMA is able to surround membrane proteins in their native lipids, producing native nanodisc SMALPs, which can then be purified and imaged (Hardy, et al., 2016; Parmar, et al., 2018). The structure of alternative complex III (ACIII) was recently solved to 3.4 Å using SMA nanodiscs (Sun, et al., 2018). Yet another method for investigating membrane protein structure uses saposins in complex with lipids and the protein of interest (Salipro, saposin-lipid-protein) (Frauenfeld, et al., 2016b; Lyons, et al., 2017). Although the process requires the membrane protein to be solubilized in detergent, reconstitution into the Salipro complex is fast and the saposin scaffold can adapt to the size

of the transmembrane region of the protein, providing a well-defined complex (Lyons, et al., 2017).

Affinity grids are a new substrate designed to selectively adsorb particles on the EM grid by applying specific affinity between substrate and sample, allowing purification steps to be combined with grid preparation. The grid has a lipid monolayer containing Ni-nitrilotriacetic acid (Ni-NTA) lipids that can recruit polyhistidine tagged (His-tagged) proteins from cell extracts, reducing the required amount of protein and time for purification (Kelly, et al., 2008). We have utilized affinity grids with His-tagged Protein A and anti-Env polyclonal antibody to study HIV CD84 virus-like particles (VLPs), resulting in less background and better control of particle density, as shown in Figure 2 (Kiss, et al., 2014). An additional affinity capture method uses 2-dimensional streptavidin crystals on a lipid monolayer as a nanosupport applied to the EM grid (Wang, et al., 2008).

Biotinylated samples may then bind the streptavidin, improving particle concentration and distribution and reducing preferred particle orientations and the structural consequences of particles binding the carbon film or colliding with the air-water interface of the sample (Wang, et al., 2008; Han, et al., 2012a; Han, et al., 2016).

Further developments of the affinity grid include the use of a NTA-PEG based coating, which combines the anti-fouling properties of brush conformation methoxypolyethylene glycol with NTA ligands on flexible PEG spacers to prevent preferred orientation of the bound His-tagged proteins (Benjamin, et al., 2016). Another example is a functionalized carbon film with covalently bound Ni-NTA, Protein G, or oligonucleotides to selectively recruit macromolecular complexes (Llaguno, et al., 2014). In a simplified affinity grid method, called cryo-Solid Phase Immune Electron Microscopy (SPIEM), antibodies or Protein A are applied directly to grids, eliminating the need to first apply a lipid monolayer (Yu, et al., 2014; Yu, et al., 2016b).

The use of the affinity capture system with silicon nitride (SiN) membrane support films has also shown promising improvements for sample preparation. The hydrophobicity of SiN supports interactions with the lipid tails of the Ni-NTA lipid monolayer, allowing for effective sample capture on the grid. Additionally, the membranes are flat, durable, and can be consistently manufactured, addressing the delicate and inconsistent nature of amorphous carbon supports (Tanner, 2013). Affinity grids combine purification steps with grid preparation, significantly reducing the time required to produce samples for cryo-EM imaging, and can be used for structure determination at high resolution. Yu *et al.* have recently used the method to determine the structure of a low concentration virus at 2.6 Å resolution (Yu, et al., 2016a).

Traditional lacey, Quantifoil (Quantifoil Micro Tools), or C-flat (Protochips, Inc) EM grids are made of a metal scaffold (e.g., copper, nickel, or gold) and an amorphous carbon support with holes of various sizes, shapes, and distributions over which the sample is suspended in vitreous ice. Irradiation of amorphous carbon in the electron microscope causes it to bend, however, leading to movement of the sample, often referred to as beam-induced motion, and therefore blurry images. Since the linear thermal expansion coefficient is much lower for

carbon than for the metal support, the carbon film may also pucker at cryo temperatures (Booy & Pawley, 1993). This can lead to poor imaging and the loss of information at high spatial frequencies. Several alternative substrates have been developed to address these deformations. Titanium-silicon metal glass films, a nanocrystalline silicon carbide substrate called Cryomesh (ProtoChips, Inc), and hydrogen-plasma treated graphene all decrease beam-induced motion, but do not completely eliminate it (Rhinow & Kuhlbrandt, 2008; Yoshioka, et al., 2010; Russo & Passmore, 2014a). Ultrastable gold substrates, which consist of a gold foil across a gold mesh grid, are one of the most promising solutions. By using the same material for the support and grid, differential thermal contraction, and therefore puckering, during cooling, is prevented and the high conductivity of gold nearly eliminates beam-induced motion, significantly improving image quality (Russo & Passmore, 2014b; Russo & Passmore, 2016a; Russo & Passmore, 2016b).

3D-DNA origami sample supports aim to address many of the current concerns for grid preparation. The sample particles are bound within a hollow support made up of double stranded DNA helices. This helps to control particle orientation, protects particles from the force of blotting with filter paper and from the air-liquid interface, and improves ice thickness consistency. The method was shown to be successful for the DNA binding protein p53, but will require more rigidity to precisely control particle orientation and will need to expand to be more widely applicable to various types of samples (Martin, et al., 2016).

Protein scaffolds are also being used to determine the structures of monomeric proteins that would otherwise be too small for cryo-EM. Coscia *et al.* have designed a self-assembled symmetric protein scaffold with a small protein genetically fused, producing a large, rigid, and symmetric particle that is more amenable to cryo-EM, and solved the structure at subnanometer resolution (Coscia, et al., 2016). Liu *et al.* have achieved near atomic resolution of a small protein called DARPIn, which is rigidly fused to a self-assembled symmetric protein cage through terminal helices. The amino acid sequence of DARPIn can be altered to tightly bind other small proteins, making it widely applicable (Liu, et al., 2018).

Cryo-EM grid ice should ideally be only slightly thicker than the sample. Excess ice thickness should be avoided because it allows the particles within an image to be at different focal heights and contributes to noise in the images (Glaeser, et al., 2016). Conventional blotting with filter paper often leads to inconsistent ice thickness and sample degradation due to the blotting force and it exposes the particles to an air-water interface of the sample. To address these problems, a “self-blotting” grid has been developed to generate reproducibly thin films of ice without the use of a filter paper blotting step (Razinkov, et al., 2016; Wei, et al., 2018). An ammonium persulfate and sodium hydroxide solution is applied to copper grids, supporting the growth of  $\text{Cu}(\text{OH})_2$  nanowires on the copper grid bars. The nanowires draw up excess liquid when the sample is applied to the grid, resulting in a thinly spread film of liquid on the grid that is then plunge frozen without the requirement of a blotting step. The self-blotting grids are used in conjunction with a newly designed freezing apparatus called the Spotiton (Jain, et al., 2012; Dandey, et al., 2018). This device uses a piezo controlled electric inkjet dispense head to deposit small volumes of sample at defined locations on the grid, which is then plunge frozen. Use of the self-blotting grid with the Spotiton results in thin films of uniform ice and the process is almost entirely automated,

increasing the reproducibility and throughput of cryo-EM grid preparation (Jain, et al., 2012; Razinkov, et al., 2016; Dandey, et al., 2018; Wei, et al., 2018).

Another blotless freezing system called the cryoWriter allows real-time monitoring of the water thickness prior to vitrification (Arnold, et al., 2017). A microcapillary is used to deposit a small sample volume (3 – 20 nanoliters) onto the grid. Depending on the volume applied, excess sample can either be recovered using the microcapillary or allowed to evaporate. The sample film is evaluated using a laser beam and photodetector and once the appropriate thickness is reached, the grid is plunge frozen. This system prevents the potentially damaging effects of filter paper blotting and uses significantly smaller volumes, allowing the investigation of low abundance samples. Methods for time resolved imaging, to capture transient states of biological molecules, by mixing reaction components immediately prior to blotting have also seen recent improvements. This was initially achieved by applying one reaction component to the EM grid in the conventional pipetting and blotting manner to achieve a thin film, then spraying another component onto the film and rapidly freezing (Berriman & Unwin, 1994; Unwin, 1995; Walker, et al., 1995; Walker, et al., 1999; Berriman & Rosenthal, 2012; Unwin & Fujiyoshi, 2012). The reaction only proceeds where the components mix, however, potentially leading to heterogeneity in the sample across the grid. This problem was addressed by coupling a micromixer with a microsyringer, allowing external homogenous mixing of the reactants before spraying onto an EM grid and plunge freezing (Lu, et al., 2009; Lu, et al., 2014b; Shaikh, et al., 2014). While this method allows the capture of dynamic processes for cryo-EM imaging, variability in ice thickness and coverage of the grid limits the regions suitable for data collection. The more recent development, by Feng *et al.*, of a polydimethylsiloxane (PDMS)-based microsyringer allows the control of ice thickness through sprayer pressure and distance from the grid, and has the potential to provide time-resolved sample preparation by mixing reactants in a channel for specified amounts of time (Feng, et al., 2017).

## Direct Electron Detectors

Low electron doses are necessary for the imaging of biological specimens in order to limit radiation damage of the sample. Cryo-EM images are therefore inherently noisy. Additionally, beam-induced motion of the sample leads to blurriness in the images. Both of these issues have been significantly improved by the development of direct electron detectors.

Several types of sensors may be used for the detection of electrons and the performance of the detector is extremely important for achieving high quality data. Detectors can be described by the detective quantum efficiency (DQE), a measure of signal produced from the sample and noise contributed to the image by the detector. A detector that contributes no noise to the image would have a DQE of 1.

Photographic film has historically been used to record cryo-EM images due to its large imaging area and high resolution. Its DQE is ~0.3-0.35 at half Nyquist frequency (McMullan, et al., 2009a; McMullan, et al., 2016). The use of film can be labor intensive and time consuming, however, as it requires development and scanning into a digital format

(Faruqi & Henderson, 2007; Binshtein & Ohi, 2015; Thompson, et al., 2016). Charge coupled device (CCD) cameras provide a much more automated mode of imaging, allowing for images to be immediately evaluated and for large datasets to be collected quickly. As the electrons hit the detector, a scintillator is used to induce the emission of photons which then hit the CCD. The photons are converted to electrical signals and an electrical charge accumulates. The charge is transferred between neighboring pixels and read out to form a digitized image (Faruqi, 1998; Sander, et al., 2005; Thompson, et al., 2016). The scintillator of a CCD camera produces electron and photon scattering, however, contributing additional noise to the images and leading to a DQE of  $\sim 0.07-0.1$  at half Nyquist frequency, significantly inferior to that of photographic film (McMullan, et al., 2009a; McMullan, et al., 2016).

Complementary metal-oxide semiconductor (CMOS) detectors are a digital alternative to CCD cameras that immediately convert charge to voltage within each pixel, so they can be operated at a high frame rate (Janesick & Putnam, 2003; Cheng, et al., 2015; Faruqi, et al., 2015). High frame rates provide the ability to fractionate the electron dose of an exposure over multiple frames. This allows the optimal use of electron dose in the image because one can compensate for the loss of high spatial frequency information as the dose accumulates. Frames can then be aligned before summing to correct for beam-induced motion and specimen drift in the image (McMullan, et al., 2014).

CMOS-based direct detection devices (DDD) have radiation hardened sensors that allow electrons to be recorded directly, rather than through a scintillator (McMullan, et al., 2009b; Guerrini, et al., 2011; Milazzo, et al., 2011). This, along with back-thinning, which decreases backscattering of electrons, results in a considerable reduction of noise in the image compared to the noise from electron and photon scattering generated in the scintillator and fiber optics of a CCD (McMullan, et al., 2009c). There are several types of DDDs that can be operated in various modes. In integration mode, charge is collected in each pixel, then integrated and read out. The DQE at half Nyquist in integration mode is  $\sim 0.4-0.6$  (McMullan, et al., 2016). In counting mode, the signal from each electron event is recorded and weighted the same, which reduces read noise and variability in electron signal. Operating in counting mode while using a high frame rate allows even higher DQEs to be achievable (Li, et al., 2013a; Li, et al., 2013b). Some cameras may additionally be operated in what is called “super-resolution” mode, in which the electron events are sub-localized within the pixel, surpassing the Nyquist frequency limit (Li, et al., 2013a; Li, et al., 2013b; Chiu, et al., 2015).

The effects of motion correction can be seen in the image of coliphage BA14 collected on a Direct Electron DE-20 (Direct Electron, LP) shown in Figure 3. The image was acquired at 12 frames per second with an exposure time of 5 seconds and then summed (Fig. 3A) or motion-corrected using scripts from Direct Electron, LP and summed (Fig. 3B). Blurring is significantly reduced by motion correction as shown in the images and power spectra. The ability to combine a high DQE with automation and the implementation of dose compensation and motion correction have led to a dramatic increase in the quality of cryo-EM data and the number of near-atomic to atomic resolution structures being determined



(Lu, et al., 2014a; Parent, et al., 2014; Voorhees, et al., 2014; Bartesaghi, et al., 2015; Hesketh, et al., 2015; von der Ecken, et al., 2015; Merk, et al., 2016).

Despite the improvements in DQE and signal-to-noise ratio provided by direct electron detectors, low contrast in cryo-EM images can still be problematic, particularly for small samples. Additional contrast enhancement, such as through the use of energy filters or phase plates, can be particularly useful in these cases.

## Phase Plates

The contrast of unstained biological materials is inherently weak under low-electron dose cryo-EM imaging conditions. Contrast can be improved by defocusing of the objective lens, although this results in a reduction of the high spatial frequency components of the image, or with the use of an energy filter, which removes inelastically scattered electrons thereby improving the signal-to-noise ratio (Langmore & Smith, 1992; Schroder, 1992). Another strategy for addressing low contrast in cryo-EM images is the use of phase plates. We have used two types of phase plates, the thin carbon-film Zernike-style phase plate and the hole-free carbon-film phase plate (HFPP), or Volta phase plate (VPP), although there are additional styles, such as electrostatic (Huang, et al., 2006; Cambie, et al., 2007; Majorovits, et al., 2007; Schultheiss, et al., 2010; Walter, et al., 2012; Frindt, et al., 2014) and magnetic phase plates (Edgcombe, et al., 2012; Blackburn & Loudon, 2014).

Zernike phase contrast (ZPC) cryo-EM uses a thin carbon film with a small hole, produced by a focused ion beam (FIB), placed in the back focal plane (Danev & Nagayama, 2008; Nagayama & Danev, 2008; Murata, et al., 2010; Schroder, 2015). Unscattered electrons pass through the hole while the scattered electrons go through the carbon film, shifting the phase of the unscattered electrons relative to the scattered electrons by  $\pi/2$ . This changes the contrast transfer function (CTF) from a sine function to a cosine function (Nagayama, 2005) and significantly improves the contrast at low spatial frequencies. The images are acquired in focus, eliminating the loss in resolution due to defocusing. The higher contrast provided by phase plates improves image alignment, making it possible for fewer particles to be averaged to produce high resolution structures by single particle analysis (Danev & Nagayama, 2008), and providing excellent results for cryo-ET (Danev, et al., 2010; Murata, et al., 2010; Guerrero-Ferreira, et al., 2011; Fukuda & Nagayama, 2012; Dai, et al., 2013). The use of ZPC cryo-EM can be challenging, however, due to a short lifespan, charging, difficulty keeping the phase plate aligned, and fringing artifacts in the images (Danev & Nagayama, 2001; Danev, et al., 2009; Fukuda, et al., 2009; Danev & Nagayama, 2010; Danev & Nagayama, 2011; Nagayama, 2011). Figure 4 illustrates the contrast provided by the Zernike-style phase plate in a tomogram of a *Caulobacter crescentus* cell infected with bacteriophage  $\phi$ CbK, as well as the fringing artifacts.

HFPP (or VPP) cryo-EM uses a homogenous carbon film in the back focal plane. Localized irradiation of the carbon film with the electron beam leads to a negative Volta potential, creating a phase shift at the position of the beam and increased contrast in the images (Danev, et al., 2014). This form of phase plate has been shown to be more stable for data collection and does not introduce strong fringing artifacts (Danev & Nagayama, 2001;

Danev & Nagayama, 2008; Danev & Nagayama, 2011; Danev, et al., 2014; Danev & Baumeister, 2016; Khoshouei, et al., 2016). It has recently been used to resolve extraordinary *in situ* detail via cryo-ET (Asano, et al., 2015; Fukuda, et al., 2015; Chlanda, et al., 2016; Mahamid, et al., 2016; Sharp, et al., 2016; Khoshouei, et al., 2017a) and to solve several high-resolution structures via single particle analysis (Chua, et al., 2016; Khoshouei, et al., 2016; Danev & Baumeister, 2017; Khoshouei, et al., 2017b). More recently, however, it has been possible to implement a slight defocus with this style of phase plate due to improvements in reconstruction software (Rohou & Grigorieff, 2015). This lessens the requirement for accuracy in focusing thus increasing the ease of use and the speed of data collection (Danev, et al., 2017; Khoshouei, et al., 2017b; Liang, et al., 2017). Processing of defocused VPP data has been shown to be either equivalent or more robust than that of defocus phase contrast cryo-EM or in-focus VPP data, by enabling the generation of 3D reconstructions using fewer particles (von Loeffelholz, et al., 2018). The use of phase plates continues to present practical challenges, however, and is generally limited to samples that are difficult to visualize without them. In Figure 5, we show 2D projection images of reovirus serotype 1 Lang (T1L) particles collected using HFPP and a slight defocus. The increased contrast allows the viral attachment fibers and released genome to be clearly resolved, without extreme fringing artifacts. Although both ZPC cryo-EM and HFPP cryo-EM provide significantly improved image contrast, the reduced fringing and relative ease of use of HFPP compared to ZPC phase plates will likely make them more widely applicable.

## Correlative Light And Electron Microscopy

Correlative Light and Electron Microscopy (CLEM or cryo-CLEM) is a technique that combines the spatiotemporal physiological information gained from fluorescence microscopy with the ever-higher resolution of structures from cryo-EM. The technique was developed in response to the absence of methods to unobtrusively label internal cell contents for cryo-EM and has been extremely useful for cellular cryo-ET studies in which localization of cellular component can be difficult in the electron microscope. The fluorescence imaging can be done live or following vitrification of the cells to capture structures in their near-native state (“LM imaging” and “cryo-CLEM imaging”, respectively, in Figure 1) (Briegel, et al., 2010). This is made possible by the introduction of cryo-cooled stages for the inverted or upright light microscope as well as the integrated light and electron microscope (Sartori, et al., 2007; Schwartz, et al., 2007; Agronskaia, et al., 2008; van Driel, et al., 2009). Several advantages of cryo-fluorescence microscopy (cryo-fLM) include the absence of morphology-altering fixation, longer fluorophor lifespan (Moerner & Orrit, 1999; Schwartz, et al., 2007; Le Gros, et al., 2009), as well as a large field of view (Rigort, et al., 2012; Bykov, et al., 2016). This allows regions of interest to be identified quickly without subjecting the sample to a lengthy screening process in the electron microscope, therefore preventing unnecessary irradiation of the sample prior to imaging. Relocating the region of interest in the electron microscope is facilitated by the use of special finder-style EM grids or commercially available fiducials such as FluoSpheres or TetraSpeck beads (100-200 nm) that are both fluorescent and electron dense (Schellenberger, et al., 2014; Schorb & Briggs, 2014). Marker-free alignment methods are also possible, as demonstrated by Anderson *et al.*,

in which the centers of the holes in the sample support are used for localization (Anderson, et al., 2018).

Samples must be relatively thin in order to be penetrable by the electron beam (less than 1  $\mu\text{m}$ ) (Al-Amoudi, et al., 2004), but must be even thinner for reliable 3D tomographic reconstruction ( $\sim 250$  nm). This is ideal for cryo-CLEM imaging of viruses (Schorb & Briggs, 2014), bacterial cells (Koning, et al., 2014; Daley, et al., 2016), or the thinnest regions of mammalian cells (van Driel, et al., 2009; Zhang, 2013; Schellenberger, et al., 2014; Carter, et al., 2018). Additional techniques, such as FIB milling to produce thin lamella (Heymann, et al., 2006; Marko, et al., 2007; Rigort, et al., 2010; Mahamid, et al., 2015; Arnold, et al., 2016; Mahamid, et al., 2016; Chaikerasitak, et al., 2017), or cryo-ultramicrotomy (CEMOVIS) (Al-Amoudi, et al., 2004; Bouchet-Marquis & Fakan, 2009; Chlanda & Sachse, 2014; Kolovou, et al., 2017), however, are required to access the interior of vitrified mammalian cells.

CLEM has been used to visualize the process of virus entry and exit from mammalian cells with great success. Using live-cell fluorescent imaging, cryo-fLM, and cryo-ET, Jun *et al.* has directly observed pseudotyped HIV-1 virions with GFP-tagged HIV-1 Vpr interacting with HeLa cells at different time points after infection (Jun, et al., 2011). Ibiricu *et al.* used live-cell fluorescence microscopy followed by cryo-ET to identify time points and location of GFP-labeled herpes simplex virus undergoing axonal transport in primary neurons cultured directly on TEM grids (Ibiricu, et al., 2011). To visualize virus after release, Strauss *et al.* used CLEM procedures to determine the arrangement of mCherry-Gag labeled HIV-1 particles anchored to cell plasma membranes via EGFP-tagged tetherin, a host cellular restriction factor that inhibits enveloped virus release, which can be seen in Figure 6 (Strauss, et al., 2016). Hampton *et al.* further investigated these tethered particles using cryo-CLEM, as shown in Figure 7 (Hampton, et al., 2017).

The latest improvements address many of the challenges associated with cryo-CLEM, such as contamination from atmospheric moisture during grid transfer steps, maintaining proper cryogenic temperatures during cryo-fLM imaging, and accurately correlating cryo-fLM and cryo-EM data. Schorb *et al.* have developed a system that optimizes grid transfer, stage stability, microscope optics, and software, establishing a comprehensive cryo-CLEM workflow (Schorb, et al., 2017). Another system by Li *et al.* uses a high-vacuum chamber on the fluorescent microscope stage, decreasing contamination of the sample and allowing the objective lens to remain at room temperature. It has additionally been adapted to use a cryo-EM holder, reducing the number of grid transfer steps (Li, et al., 2018). Future developments in CLEM will expand the use of cryo-super-resolution microscopy to localize specific proteins, further bridging the gap in resolution between light and electron microscopy (Chang, et al., 2014; Kaufmann, et al., 2014; Liu, et al., 2015; Kaufmann, et al., 2016; Wolf, et al., 2016).

## Conclusions and Outlook

Since its development, cryo-EM has played an important role in structural biology and is contributing more and more with recent advances. New developments are broadening the

cryo-EM spectrum from whole cells to peptides, allowing more biological questions of greater complexity to be answered and there is still room for improvement.

The timing and capturing of rare and specific events on the macromolecular and cellular levels is now possible using microsyringes and CLEM, respectively, for time-resolved imaging. Reproducibility in the sample preparation and grid preparation processes should continue to improve as grid-based purification methods and the development of vitrification devices such as the Spotiton and cryoWriter mature and expand. Beam-induced motion is being addressed both by the grid substrate and through the use of correction algorithms that utilize the high-frame rate of direct electron detectors.

Advances in electron detection over the past several years have provided remarkable improvements for cryo-EM data collection and quality. Further increasing frame rates, the use of counting mode on all systems, and increased pixel sizes will provide even higher DQEs and super resolution mode should allow direct electron detectors to be used beyond Nyquist frequency (McMullan, et al., 2016).

While phase plates have shown extraordinary promise for cryo-EM, there are still improvements that can be made. Usage is generally limited to those with expertise (Danev & Nagayama, 2008; Glaeser, et al., 2013; Subramaniam, et al., 2016) and takes a considerable amount of time, so workflow development will be incredibly important for more widespread implementation. Higher reproducibility in the manufacture of phase plates and methods for evaluating phase plate quality during use will also prove to be useful. Phase plates should allow increasingly higher resolution structural work, particularly for small samples, and for entire datasets to be collected more quickly since fewer images will be required.

As CLEM continues to develop, labeling strategies that are retained between live cell and cryo-EM imaging will allow more and more complex biological questions to be addressed and simultaneously fluorescent and electron-dense markers will aid in more precise correlation between light and electron microscopy. Combining cryo-FIB milling of cryo-samples with cryo-CLEM will provide a method for thicker specimens to be investigated and improvements to sample stability between steps of the workflow will help the process become more user-friendly.

The recent developments in cryo-EM imaging, along with improvements in image processing, have allowed tremendous growth in the field over the last few years. We expect this expansion to continue, with cryo-EM providing structures to higher resolutions and answers to increasingly intricate biological questions.

## Supplementary Material

Refer to Web version on PubMed Central for supplementary material.

## Acknowledgments

### FUNDING INFORMATION

The authors acknowledge the Robert P. Apkarian Integrated Electron Microscopy Core of Emory University for microscopy services and support. We would like to thank Prof. Xuemin Chen for the HIV-1 VLPs, Prof. Bernardo Mainou for the reovirus T1L preparation, and Prof. Ian Molineux for providing us with coliphage BA14. This work was supported in part by Emory University, Children's Healthcare of Atlanta, and the Georgia Research Alliance to E.R.W.; the Center for AIDS Research at Emory University (P30 AI050409); the James B. Pendleton Charitable Trust to E.R.W.; public health service grants R01GM104540, R01GM114561, R21AI101775, R01GM104540-03S1 to E.R.W. from the NIH, and NSF grant 0923395 to E.R.W. Public health service grant F32GM112517 to J.D.S. from the NIH. Reovirus data collection at Florida State University was made possible by NIH grants S10 OD018142-01, S10 RR025080-01, and U24 GM116788 to K. A. T.

## References

- Adrian M, Dubochet J, Lepault J, McDowell AW. Cryo-electron microscopy of viruses. *Nature*. 1984; 308(5954):32–36. [PubMed: 6322001]
- Agafonov DE, Kastner B, Dybkov O, Hofele RV, Liu WT, Urlaub H, Luhrmann R, Stark H. Molecular architecture of the human U4/U6.U5 tri-snRNP. *Science*. 2016; 351(6280):1416–1420. [PubMed: 26912367]
- Agronskaia AV, Valentijn JA, van Driel LF, Schneijdenberg CT, Humbel BM, van Bergen en Henegouwen PM, Verkleij AJ, Koster AJ, Gerritsen HC. Integrated fluorescence and transmission electron microscopy. *J Struct Biol*. 2008; 164(2):183–189. [PubMed: 18664385]
- Al-Amoudi A, Chang JJ, Leforestier A, McDowell A, Salamin LM, Norlen LP, Richter K, Blanc NS, Studer D, Dubochet J. Cryo-electron microscopy of vitreous sections. *EMBO J*. 2004; 23(18):3583–3588. [PubMed: 15318169]
- Althoff T, Mills DJ, Popot J-L, Kühlbrandt W. Arrangement of electron transport chain components in bovine mitochondrial supercomplex I(1)III(2)IV(1). *EMBO J*. 2011; 30(22):4652–4664. [PubMed: 21909073]
- Anderson KL, Page C, Swift MF, Hanein D, Volkman N. Marker-free method for accurate alignment between correlated light, cryo-light, and electron cryo-microscopy data using sample support features. *J Struct Biol*. 2018; 201(1):46–51. [PubMed: 29113849]
- Arnold J, Mahamid J, Lucic V, de Marco A, Fernandez J-J, Laugks T, Mayer T, Hyman Anthony A, Baumeister W, Plitzko Jürgen M. Site-Specific Cryo-focused Ion Beam Sample Preparation Guided by 3D Correlative Microscopy. *Biophys J*. 2016; 110(4):860–869. [PubMed: 26769364]
- Arnold SA, Albiez S, Bieri A, Syntychaki A, Adaixo R, McLeod RA, Goldie KN, Stahlberg H, Braun T. Blotting-free and lossless cryo-electron microscopy grid preparation from nanoliter-sized protein samples and single-cell extracts. *J Struct Biol*. 2017; 197(3):220–226. [PubMed: 27864160]
- Asano S, Fukuda Y, Beck F, Aufderheide A, Forster F, Danev R, Baumeister W. Proteasomes. A molecular census of 26S proteasomes in intact neurons. *Science*. 2015; 347(6220):439–442. [PubMed: 25613890]
- Bai X-C, McMullan G, Scheres SHW. How cryo-EM is revolutionizing structural biology. *Trends Biochem Sci*. 2015; 40(1):49–57. [PubMed: 25544475]
- Baker MR, Fan G, Serysheva II. Single-particle cryo-EM of the ryanodine receptor channel in an aqueous environment. *Eur J Transl Myol*. 2015; 25(1):35–48. [PubMed: 25844145]
- Bartesaghi A, Merk A, Banerjee S, Matthies D, Wu X, Milne JL, Subramaniam S. 2.2 Å resolution cryo-EM structure of beta-galactosidase in complex with a cell-permeant inhibitor. *Science*. 2015; 348(6239):1147–1151. [PubMed: 25953817]
- Benjamin CJ, Wright KJ, Hyun SH, Krynski K, Yu G, Bajaj R, Guo F, Stauffacher CV, Jiang W, Thompson DH. Nonfouling NTA-PEG-Based TEM Grid Coatings for Selective Capture of Histidine-Tagged Protein Targets from Cell Lysates. *Langmuir*. 2016; 32(2):551–559. [PubMed: 26726866]
- Berriman J, Unwin N. Analysis of transient structures by cryo-microscopy combined with rapid mixing of spray droplets. *Ultramicroscopy*. 1994; 56(4):241–252. [PubMed: 7831735]
- Berriman JA, Rosenthal PB. Paraxial charge compensator for electron cryomicroscopy. *Ultramicroscopy*. 2012; 116:106–114. [PubMed: 22564508]
- Bertram K, Agafonov DE, Liu WT, Dybkov O, Will CL, Hartmuth K, Urlaub H, Kastner B, Stark H, Luhrmann R. Cryo-EM structure of a human spliceosome activated for step 2 of splicing. *Nature*. 2017; 542(7641):318. + [PubMed: 28076346]

- Binshtein E, Ohi MD. Cryo-electron microscopy and the amazing race to atomic resolution. *Biochemistry*. 2015; 54(20):3133–3141. [PubMed: 25955078]
- Blackburn AM, Loudon JC. Vortex beam production and contrast enhancement from a magnetic spiral phase plate. *Ultramicroscopy*. 2014; 136:127–143. [PubMed: 24128851]
- Booy FP, Pawley JB. Cryo-crinkling: what happens to carbon films on copper grids at low temperature. *Ultramicroscopy*. 1993; 48(3):273–280. [PubMed: 8475597]
- Bouchet-Marquis C, Fakan S. Cryoelectron microscopy of vitreous sections: a step further towards the native state. *Methods Mol Biol*. 2009; 464:425–439. [PubMed: 18951199]
- Briegel A, Chen S, Koster AJ, Plitzko JM, Schwartz CL, Jensen GJ. Chapter Thirteen - Correlated Light and Electron Cryo-Microscopy. In: Jensen GJ, editor *Methods Enzymol*. Academic Press; 2010. 317–341.
- Brilot AF, Chen JZ, Cheng A, Pan J, Harrison SC, Potter CS, Carragher B, Henderson R, Grigorieff N. Beam-Induced Motion of Vitrified Specimen on Holey Carbon Film. *J Struct Biol*. 2012; 177(3): 630–637. [PubMed: 22366277]
- Bykov YS, Cortese M, Briggs JAG, Bartschlager R. Correlative light and electron microscopy methods for the study of virus-cell interactions. *FEBS Lett*. 2016; 590(13):1877–1895. [PubMed: 27008928]
- Cambie R, Downing KH, Typke D, Glaeser RM, Jin J. Design of a microfabricated, two-electrode phase-contrast element suitable for electron microscopy. *Ultramicroscopy*. 2007; 107(4–5):329–339. [PubMed: 17079082]
- Cao E, Liao M, Cheng Y, Julius D. TRPV1 structures in distinct conformations reveal mechanisms of activation. *Nature*. 2013; 504(7478):113–118. [PubMed: 24305161]
- Carter SD, Mageswaran SK, Farino ZJ, Mamede JI, Oikonomou CM, Hope TJ, Freyberg Z, Jensen GJ. Distinguishing signal from autofluorescence in cryogenic correlated light and electron microscopy of mammalian cells. *J Struct Biol*. 2018; 201(1):15–25. [PubMed: 29078993]
- Chaikeeratisak V, Nguyen K, Khanna K, Brilot AF, Erb ML, Coker JK, Vavilina A, Newton GL, Buschauer R, Pogliano K, Villa E, Agard DA, Pogliano J. Assembly of a nucleus-like structure during viral replication in bacteria. *Science*. 2017; 355(6321):194–197. [PubMed: 28082593]
- Chang Y-W, Chen S, Tocheva EI, Treuner-Lange A, Löbach S, Søggaard-Andersen L, Jensen GJ. Correlated cryogenic photoactivated localization microscopy and cryo-electron tomography. *Nat Methods*. 2014; 11:737. [PubMed: 24813625]
- Cheng Y, Grigorieff N, Penczek PA, Walz T. A primer to single-particle cryo-electron microscopy. *Cell*. 2015; 161(3):438–449. [PubMed: 25910204]
- Chiu P-L, Li X, Li Z, Beckett B, Brilot AF, Grigorieff N, Agard DA, Cheng Y, Walz T. Evaluation of super-resolution performance of the K2 electron-counting camera using 2D crystals of aquaporin-0. *J Struct Biol*. 2015; 192(2):163–173. [PubMed: 26318383]
- Chlanda P, Mekhedov E, Waters H, Schwartz CL, Fischer ER, Ryham RJ, Cohen FS, Blank PS, Zimmerberg J. The hemifusion structure induced by influenza virus haemagglutinin is determined by physical properties of the target membranes. *Nat Microbiol*. 2016; 1(6):16050. [PubMed: 27572837]
- Chlanda P, Sachse M. Cryo-electron microscopy of vitreous sections. *Methods Mol Biol*. 2014; 1117:193–214. [PubMed: 24357365]
- Chowdhury S, Ketcham SA, Schroer TA, Lander GC. Structural organization of the dynein-dynactin complex bound to microtubules. *Nat Struct Mol Biol*. 2015; 22(4):345–347. [PubMed: 25751425]
- Chua EY, Vogirala VK, Inian O, Wong AS, Nordenskiöld L, Plitzko JM, Danev R, Sandin S. 3.9 Å structure of the nucleosome core particle determined by phase-plate cryo-EM. *Nucleic Acids Res*. 2016; 44(17):8013–8019. [PubMed: 27563056]
- Coscia F, Estrozi LF, Hans F, Malet H, Noirclerc-Savoie M, Schoehn G, Petosa C. Fusion to a homo-oligomeric scaffold allows cryo-EM analysis of a small protein. *Sci Rep*. 2016; 6:30909. [PubMed: 27485862]
- Cvetkov TL, Huynh KW, Cohen MR, Moiseenkova-Bell VY. Molecular Architecture and Subunit Organization of TRPA1 Ion Channel Revealed by Electron Microscopy. *J Biol Chem*. 2011; 286(44):38168–38176. [PubMed: 21908607]

- Dahl R, Staehelin LA. High-pressure freezing for the preservation of biological structure: theory and practice. *J Electron Microscop Tech.* 1989; 13(3):165–174. [PubMed: 2685196]
- Dai W, Fu C, Raytcheva D, Flanagan J, Khant HA, Liu X, Rochat RH, Haase-Pettingell C, Piret J, Ludtke SJ, Nagayama K, Schmid MF, King JA, Chiu W. Visualizing Virus Assembly Intermediates Inside Marine Cyanobacteria. *Nature.* 2013; 502(7473):707–710. [PubMed: 24107993]
- Daley DO, Skoglund U, Söderström B. FtsZ does not initiate membrane constriction at the onset of division. *Sci Rep.* 2016; 6:33138. [PubMed: 27609565]
- Dandey VP, Wei H, Zhang Z, Tan YZ, Acharya P, Eng ET, Rice WJ, Kahn PA, Potter CS, Carragher B. Spotiton: New features and applications. *J Struct Biol.* 2018
- Danev R, Baumeister W. Cryo-EM single particle analysis with the Volta phase plate. *eLife.* 2016; 5
- Danev R, Baumeister W. Expanding the boundaries of cryo-EM with phase plates. *Curr Opin Struct Biol.* 2017; 46:87–94. [PubMed: 28675816]
- Danev R, Buijsse B, Khoshouei M, Plitzko JM, Baumeister W. Volta potential phase plate for in-focus phase contrast transmission electron microscopy. *Proc Natl Acad Sci U S A.* 2014; 111(44): 15635–15640. [PubMed: 25331897]
- Danev R, Glaeser RM, Nagayama K. Practical factors affecting the performance of a thin-film phase plate for transmission electron microscopy. *Ultramicroscopy.* 2009; 109(4):312–325. [PubMed: 19157711]
- Danev R, Kanamaru S, Marko M, Nagayama K. Zernike phase contrast cryo-electron tomography. *J Struct Biol.* 2010; 171(2):174–181. [PubMed: 20350600]
- Danev R, Nagayama K. Transmission electron microscopy with Zernike phase plate. *Ultramicroscopy.* 2001; 88(4):243–252. [PubMed: 11545320]
- Danev R, Nagayama K. Single particle analysis based on Zernike phase contrast transmission electron microscopy. *J Struct Biol.* 2008; 161(2):211–218. [PubMed: 18082423]
- Danev R, Nagayama K. Phase plates for transmission electron microscopy. *Methods Enzymol.* 2010; 481:343–369. [PubMed: 20887864]
- Danev R, Nagayama K. Optimizing the phase shift and the cut-on periodicity of phase plates for TEM. *Ultramicroscopy.* 2011; 111(8):1305–1315. [PubMed: 21864771]
- Danev R, Tegenov D, Baumeister W. Using the Volta phase plate with defocus for cryo-EM single particle analysis. *eLife.* 2017; 6
- Doerr A. Single-particle cryo-electron microscopy. *Nat Methods.* 2015; 13:23.
- Dubochet J. High-pressure freezing for cryoelectron microscopy. *Trends Cell Biol.* 1995; 5(9):366–368. [PubMed: 14732080]
- Dubochet J, Adrian M, Chang JJ, Homo JC, Lepault J, McDowell AW, Schultz P. Cryo-electron microscopy of vitrified specimens. *Q Rev Biophys.* 1988; 21(2):129–228. [PubMed: 3043536]
- Dubochet J, McDowell AW, Menge B, Schmid EN, Lickfeld KG. Electron microscopy of frozen-hydrated bacteria. *J Bacteriol.* 1983; 155(1):381–390. [PubMed: 6408064]
- Edgcombe CJ, Ionescu A, Loudon JC, Blackburn AM, Kurebayashi H, Barnes CHW. Characterisation of ferromagnetic rings for Zernike phase plates using the Aharonov-Bohm effect. *Ultramicroscopy.* 2012; 120:78–85. [PubMed: 22842114]
- Efremov RG, Gatsogiannis C, Raunser S. Chapter One - Lipid Nanodiscs as a Tool for High-Resolution Structure Determination of Membrane Proteins by Single-Particle Cryo-EM. In: Ziegler C, editor *Methods Enzymol.* Academic Press; 2017. 1–30.
- Efremov RG, Leitner A, Aebersold R, Raunser S. Architecture and conformational switch mechanism of the ryanodine receptor. *Nature.* 2015; 517:39. [PubMed: 25470059]
- Faruqi AR. Design principles and applications of a cooled CCD camera for electron microscopy. *Adv Exp Med Biol.* 1998; 453:63–72. [PubMed: 9889815]
- Faruqi AR, Henderson R. Electronic detectors for electron microscopy. *Curr Opin Struct Biol.* 2007; 17(5):549–555. [PubMed: 17913494]
- Faruqi AR, Henderson R, McMullan G. Chapter Two - Progress and Development of Direct Detectors for Electron Cryomicroscopy. In: Hawkes PW, editor *Adv Imaging Electron Phys.* Elsevier; 2015. 103–141.

- Feng X, Fu Z, Kaledhonkar S, Jia Y, Shah B, Jin A, Liu Z, Sun M, Chen B, Grassucci RA, Ren Y, Jiang H, Frank J, Lin Q. A Fast and Effective Microfluidic Spraying-Plunging Method for High-Resolution Single-Particle Cryo-EM. *Structure*. 2017; 25(4):663–670.e663. [PubMed: 28286002]
- Fernandez-Leiro R, Scheres SHW. Unravelling biological macromolecules with cryo-electron microscopy. *Nature*. 2016; 537:339. [PubMed: 27629640]
- Fiedorczuk K, Letts JA, Degliesposti G, Kaszuba K, Skehel M, Sazanov LA. Atomic structure of the entire mammalian mitochondrial complex I. *Nature*. 2016; 538(7625):406. + [PubMed: 27595392]
- Flötenmeyer M, Weiss H, Tribet C, Popot J-L, Leonard K. The use of amphipathic polymers for cryo electron microscopy of NADH:ubiquinone oxidoreductase (complex I). *J Microsc*. 2007; 227(3): 229–235. [PubMed: 17760617]
- Frank J. Advances in the field of single-particle cryo-electron microscopy over the last decade. *Nat Protoc*. 2017; 12:209. [PubMed: 28055037]
- Frauenfeld J, Gumbart J, van der Sluis EO, Funes S, Gartmann M, Beatrix B, Mielke T, Berninghausen O, Becker T, Schulten K, Beckmann R. Cryo-EM structure of the ribosome-SecYE complex in the membrane environment. *Nat Struct Mol Biol*. 2011; 18(5):614–621. [PubMed: 21499241]
- Frauenfeld J, Löving R, Armache J-P, Sonnen A, Guettou F, Moberg P, Zhu L, Jegerschöld C, Flayhan A, Briggs JAG, Garoff H, Löw C, Cheng Y, Nordlund P. A novel lipoprotein nanoparticle system for membrane proteins. *Nat Methods*. 2016a; 13(4):345–351. [PubMed: 26950744]
- Frauenfeld J, Löving R, Armache J-P, Sonnen AFP, Guettou F, Moberg P, Zhu L, Jegerschöld C, Flayhan A, Briggs JAG, Garoff H, Löw C, Cheng Y, Nordlund P. A saposin-lipoprotein nanoparticle system for membrane proteins. *Nat Methods*. 2016b; 13:345. [PubMed: 26950744]
- Frindt N, Oster M, Hettler S, Gamm B, Dieterle L, Kowalsky W, Gerthsen D, Schröder RR. In-Focus Electrostatic Zach Phase Plate Imaging for Transmission Electron Microscopy with Tunable Phase Contrast of Frozen Hydrated Biological Samples. *Microsc Microanal*. 2014; 20(1):175–183. [PubMed: 24382158]
- Fukuda Y, Fukazawa Y, Danev R, Shigemoto R, Nagayama K. Tuning of the Zernike phase-plate for visualization of detailed ultrastructure in complex biological specimens. *J Struct Biol*. 2009; 168(3):476–484. [PubMed: 19732832]
- Fukuda Y, Laugks U, Lucic V, Baumeister W, Danev R. Electron cryotomography of vitrified cells with a Volta phase plate. *J Struct Biol*. 2015; 190(2):143–154. [PubMed: 25770733]
- Fukuda Y, Nagayama K. Zernike phase contrast cryo-electron tomography of whole mounted frozen cells. *J Struct Biol*. 2012; 177(2):484–489. [PubMed: 22119892]
- Gao Y, Cao E, Julius D, Cheng Y. TRPV1 structures in nanodiscs reveal mechanisms of ligand and lipid action. *Nature*. 2016; 534:347. [PubMed: 27281200]
- Gatsogiannis C, Merino F, Prumbaum D, Roderer D, Leidreiter F, Meusch D, Raunser S. Membrane insertion of a Tc toxin in near-atomic detail. *Nat Struct Mol Biol*. 2016; 23:884. [PubMed: 27571177]
- Glaeser RM, Han BG, Csencsits R, Killilea A, Pulk A, Cate JH. Factors that Influence the Formation and Stability of Thin, Cryo-EM Specimens. *Biophys J*. 2016; 110(4):749–755. [PubMed: 26386606]
- Glaeser RM, McMullan G, Faruqi AR, Henderson R. Images of paraffin monolayer crystals with perfect contrast: minimization of beam-induced specimen motion. *Ultramicroscopy*. 2011; 111(2): 90–100. [PubMed: 21185452]
- Glaeser RM, Sassolini S, Cambie R, Jin J, Cabrini S, Schmid AK, Danev R, Buijsse B, Csencsits R, Downing KH, Larson DM, Typke D, Han BG. Minimizing electrostatic charging of an aperture used to produce in-focus phase contrast in the TEM. *Ultramicroscopy*. 2013; 135:6–15. [PubMed: 23872037]
- Grabenbauer M, Han HM, Huebinger J. Cryo-fixation by self-pressurized rapid freezing. *Methods Mol Biol*. 2014; 1117:173–191. [PubMed: 24357364]
- Guerrero-Ferreira RC, Viollier PH, Ely B, Poindexter JS, Georgieva M, Jensen GJ, Wright ER. Alternative mechanism for bacteriophage adsorption to the motile bacterium *Caulobacter crescentus*. *Proc Natl Acad Sci U S A*. 2011; 108(24):9963. [PubMed: 21613567]
- Guerrini N, Turchetta R, Hoftens GV, Henderson R, McMullan G, Faruqi AR. A high frame rate, 16 million pixels, radiation hard CMOS sensor. *Journal of Instrumentation*. 2011; 6(03):C03003.



- Guo F, Jiang W. Single Particle Cryo-electron Microscopy and 3-D Reconstruction of Viruses. *Methods Mol Biol.* 2014; 1117:401–443. [PubMed: 24357374]
- Hampton CM, Strauss JD, Ke Z, Dillard RS, Hammonds JE, Alonas E, Desai TM, Marin M, Storms RE, Leon F, Melikyan GB, Santangelo PJ, Spearman PW, Wright ER. Correlated fluorescence microscopy and cryo-electron tomography of virus-infected or transfected mammalian cells. *Nat Protoc.* 2017; 12(1):150–167. [PubMed: 27977021]
- Han B-G, Watson Z, Kang H, Pulk A, Downing KH, Cate J, Glaeser RM. Long shelf-life streptavidin support-films suitable for electron microscopy of biological macromolecules. *J Struct Biol.* 2016; 195(2):238–244. [PubMed: 27320699]
- Han BG, Walton RW, Song A, Hwu P, Stubbs MT, Yannone SM, Arbelaez P, Dong M, Glaeser RM. Electron microscopy of biotinylated protein complexes bound to streptavidin monolayer crystals. *J Struct Biol.* 2012a; 180(1):249–253. [PubMed: 22584152]
- Han H-M, Huebinger J, Grabenbauer M. Self-pressurized rapid freezing (SPRF) as a simple fixation method for cryo-electron microscopy of vitreous sections. *J Struct Biol.* 2012b; 178(2):84–87. [PubMed: 22508105]
- Hardy D, Bill Roslyn M, Jawhari A, Rothnie Alice J. Overcoming bottlenecks in the membrane protein structural biology pipeline. *Biochem Soc Trans.* 2016; 44(3):838. [PubMed: 27284049]
- Hesketh EL, Meshcheriakova Y, Dent KC, Saxena P, Thompson RF, Cockburn JJ, Lomonosoff GP, Ranson NA. Mechanisms of assembly and genome packaging in an RNA virus revealed by high-resolution cryo-EM. *Nat Commun.* 2015; 6:10113. [PubMed: 26657148]
- Hewat EA, Neumann E. Characterization of the performance of a 200-kV field emission gun for cryo-electron microscopy of biological molecules. *J Struct Biol.* 2002; 139(1):60–64. [PubMed: 12372321]
- Heymann JA, Hayles M, Gestmann I, Giannuzzi LA, Lich B, Subramaniam S. Site-specific 3D imaging of cells and tissues with a dual beam microscope. *J Struct Biol.* 2006; 155(1):63–73. [PubMed: 16713294]
- Huang SH, Wang WJ, Chang CS, Hwu YK, Tseng FG, Kai JJ, Chen FR. The fabrication and application of Zernike electrostatic phase plate. *J Electron Microsc (Tokyo).* 2006; 55(6):273–280. [PubMed: 17223649]
- Ibiricu I, Huiskonen JT, Dohner K, Bradke F, Sodeik B, Grünewald K. Cryo electron tomography of herpes simplex virus during axonal transport and secondary envelopment in primary neurons. *PLoS Pathog.* 2011; 7(12):e1002406. [PubMed: 22194682]
- Jain T, Sheehan P, Crum J, Carragher B, Potter CS. Spotiton: a prototype for an integrated inkjet dispense and vitrification system for cryo-TEM. *J Struct Biol.* 2012; 179(1):68–75. [PubMed: 22569522]
- Janesick J, Putnam G. DEVELOPMENTS AND APPLICATIONS OF HIGHPERFORMANCE CCD AND CMOS IMAGING ARRAYS. *Annual Review of Nuclear and Particle Science.* 2003; 53(1): 263–300.
- Jin P, Bulkley D, Guo Y, Zhang W, Guo Z, Huynh W, Wu S, Meltzer S, Cheng T, Jan LY, Jan Y-N, Cheng Y. Cryo-EM Structure of the Mechanotransduction Channel NOMPC. *Nature.* 2017; 547(7661):118–122. [PubMed: 28658211]
- Jun S, Ke D, Debiec K, Zhao G, Meng X, Ambrose Z, Gibson GA, Watkins SC, Zhang P. Direct visualization of HIV-1 with correlative live-cell microscopy and cryo-electron tomography. *Structure.* 2011; 19(11):1573–1581. [PubMed: 22078557]
- Kastner B, Fischer N, Golas MM, Sander B, Dube P, Boehringer D, Hartmuth K, Deckert J, Hauer F, Wolf E, Uchtenhagen H, Urlaub H, Herzog F, Peters JM, Poerschke D, Luhrmann R, Stark H. GraFix: sample preparation for single-particle electron cryomicroscopy. *Nat Methods.* 2008; 5(1): 53–55. [PubMed: 18157137]
- Kaufmann R, Hagen C, Grünewald K. *European Microscopy Congress 2016: Proceedings.* Wiley-VCH Verlag GmbH & Co. KGaA; 2016. Super-resolution fluorescence microscopy of cryo-immobilized samples.
- Kaufmann R, Schellenberger P, Seiradake E, Dobbie IM, Jones EY, Davis I, Hagen C, Grünewald K. Super-Resolution Microscopy Using Standard Fluorescent Proteins in Intact Cells under Cryo-Conditions. *Nano Lett.* 2014; 14(7):4171–4175. [PubMed: 24884378]

- Kelly DF, Abeyrathne PD, Dukovski D, Walz T. The Affinity Grid: a pre-fabricated EM grid for monolayer purification. *J Mol Biol.* 2008; 382(2):423–433. [PubMed: 18655791]
- Khoshouei M, Pfeffer S, Baumeister W, Forster F, Danev R. Subtomogram analysis using the Volta phase plate. *J Struct Biol.* 2017a; 197(2):94–101. [PubMed: 27235783]
- Khoshouei M, Radjainia M, Baumeister W, Danev R. Cryo-EM structure of haemoglobin at 3.2 Å determined with the Volta phase plate. *Nat Commun.* 2017b; 8:16099. [PubMed: 28665412]
- Khoshouei M, Radjainia M, Phillips AJ, Gerrard JA, Mitra AK, Plitzko JM, Baumeister W, Danev R. Volta phase plate cryo-EM of the small protein complex Prx3. *Nat Commun.* 2016; 7:10534. [PubMed: 26817416]
- Kiss G, Chen X, Brindley MA, Campbell P, Afonso CL, Ke Z, Holl JM, Guerrero-Ferreira RC, Byrd-Leotis LA, Steel J, Steinhauer DA, Plemper RK, Kelly DF, Spearman PW, Wright ER. Capturing enveloped viruses on affinity grids for downstream cryo-electron microscopy applications. *Microsc Microanal.* 2014; 20(1):164–174. [PubMed: 24279992]
- Kolovou A, Schorb M, Tarafder A, Sachse C, Schwab Y, Santarella-Mellwig R. A new method for cryo-sectioning cell monolayers using a correlative workflow. *Methods Cell Biol.* 2017; 140:85–103. [PubMed: 28528643]
- Koning RI, Celler K, Willemse J, Bos E, van Wezel GP, Koster AJ. Chapter 10 - Correlative Cryo-Fluorescence Light Microscopy and Cryo-Electron Tomography of *Streptomyces*. In: Müller-Reichert T, Verkade P, editors *Methods Cell Biol.* Academic Press; 2014. 217–239.
- Kosinski J, Mosalaganti S, von Appen A, Teimer R, DiGuilio AL, Wan W, Bui KH, Hagen WJH, Briggs JAG, Glavy JS, Hurt E, Beck M. Molecular architecture of the inner ring scaffold of the human nuclear pore complex. *Science.* 2016; 352(6283):363–365. [PubMed: 27081072]
- Kuhlbrandt W. Biochemistry. The resolution revolution. *Science.* 2014; 343(6178):1443–1444. [PubMed: 24675944]
- Langmore JP, Smith MF. Quantitative energy-filtered electron microscopy of biological molecules in ice. *Ultramicroscopy.* 1992; 46(1–4):349–373. [PubMed: 1336234]
- Lasker K, Forster F, Bohn S, Walzthoeni T, Villa E, Unverdorben P, Beck F, Aebersold R, Sali A, Baumeister W. Molecular architecture of the 26S proteasome holocomplex determined by an integrative approach. *Proc Natl Acad Sci U S A.* 2012; 109(5):1380–1387. [PubMed: 22307589]
- Le Gros MA, McDermott G, Uchida M, Knoechel CG, Larabell CA. High-aperture cryogenic light microscopy. *J Microsc.* 2009; 235(1):1–8. [PubMed: 19566622]
- Lepault J, Booy FP, Dubochet J. Electron microscopy of frozen biological suspensions. *J Microsc.* 1983; 129(Pt 1):89–102. [PubMed: 6186816]
- Leunissen JL, Yi H. Self-pressurized rapid freezing (SPRF): a novel cryofixation method for specimen preparation in electron microscopy. *J Microsc.* 2009; 235(1):25–35. [PubMed: 19566624]
- Li S, Ji G, Shi Y, Klausen LH, Niu T, Wang S, Huang X, Ding W, Zhang X, Dong M, Xu W, Sun F. High-vacuum optical platform for cryo-CLEM (HOPE): A new solution for non-integrated multiscale correlative light and electron microscopy. *J Struct Biol.* 2018; 201(1):63–75. [PubMed: 29113848]
- Li X, Mooney P, Zheng S, Booth CR, Braunfeld MB, Gubbens S, Agard DA, Cheng Y. Electron counting and beam-induced motion correction enable near-atomic-resolution single-particle cryo-EM. *Nat Methods.* 2013a; 10(6):584–590. [PubMed: 23644547]
- Li X, Zheng SQ, Egami K, Agard DA, Cheng Y. Influence of electron dose rate on electron counting images recorded with the K2 camera. *J Struct Biol.* 2013b; 184(2):251–260. [PubMed: 23968652]
- Liang YL, Khoshouei M, Radjainia M, Zhang Y, Glukhova A, Tarrasch J, Thal DM, Furness SGB, Christopoulos G, Coudrat T, Danev R, Baumeister W, Miller LJ, Christopoulos A, Kobilka BK, Wooten D, Skiniotis G, Sexton PM. Phase-plate cryo-EM structure of a class B GPCR-G-protein complex. *Nature.* 2017; 546(7656):118–123. [PubMed: 28437792]
- Liao M, Cao E, Julius D, Cheng Y. Structure of the TRPV1 ion channel determined by electron cryo-microscopy. *Nature.* 2013; 504(7478):107–112. [PubMed: 24305160]
- Linke D. Detergents: an overview. *Methods Enzymol.* 2009; 463:603–617. [PubMed: 19892194]

- Liu B, Xue Y, Zhao W, Chen Y, Fan C, Gu L, Zhang Y, Zhang X, Sun L, Huang X, Ding W, Sun F, Ji W, Xu T. Three-dimensional superresolution protein localization correlated with vitrified cellular context. *Sci Rep.* 2015; 5:13017. [PubMed: 26462878]
- Liu Y, Gonen S, Gonen T, Yeates TO. Near-atomic cryo-EM imaging of a small protein displayed on a designed scaffolding system. *Proc Natl Acad Sci U S A.* 2018
- Llaguno MC, Xu H, Shi L, Huang N, Zhang H, Liu Q, Jiang QX. Chemically functionalized carbon films for single molecule imaging. *J Struct Biol.* 2014; 185(3):405–417. [PubMed: 24457027]
- Lu P, Bai XC, Ma D, Xie T, Yan C, Sun L, Yang G, Zhao Y, Zhou R, Scheres SH, Shi Y. Three-dimensional structure of human gamma-secretase. *Nature.* 2014a; 512(7513):166–170. [PubMed: 25043039]
- Lu Z, Barnard D, Shaikh TR, Meng X, Mannella CA, Yassin A, Agrawal R, Wagenknecht T, Lu TM. Gas-Assisted Annular Microsprayer for Sample Preparation for Time-Resolved Cryo-Electron Microscopy. *J Micromech Microeng.* 2014b; 24(11):115001. [PubMed: 25530679]
- Lu Z, Shaikh TR, Barnard D, Meng X, Mohamed H, Yassin A, Mannella CA, Agrawal RK, Lu TM, Wagenknecht T. Monolithic microfluidic mixing-spraying devices for time-resolved cryo-electron microscopy. *J Struct Biol.* 2009; 168(3):388–395. [PubMed: 19683579]
- Lyons JA, Bøggild A, Nissen P, Frauenfeld J. Chapter Three - Saposin-Lipoprotein Scaffolds for Structure Determination of Membrane Transporters. In: Ziegler C, editor *Methods Enzymol.* Academic Press; 2017. 85–99.
- Lyumkis D, Julien JP, de Val N, Cupo A, Potter CS, Klasse PJ, Burton DR, Sanders RW, Moore JP, Carragher B, Wilson IA, Ward AB. Cryo-EM structure of a fully glycosylated soluble cleaved HIV-1 envelope trimer. *Science.* 2013; 342(6165):1484–1490. [PubMed: 24179160]
- Mahamid J, Pfeffer S, Schaffer M, Villa E, Danev R, Cuellar LK, Forster F, Hyman AA, Plitzko JM, Baumeister W. Visualizing the molecular sociology at the HeLa cell nuclear periphery. *Science.* 2016; 351(6276):969–972. [PubMed: 26917770]
- Mahamid J, Schampers R, Persoon H, Hyman AA, Baumeister W, Plitzko JM. A focused ion beam milling and lift-out approach for site-specific preparation of frozen-hydrated lamellas from multicellular organisms. *J Struct Biol.* 2015; 192(2):262–269. [PubMed: 26216184]
- Majorovits E, Barton B, Schultheiss K, Perez-Willard F, Gerthsen D, Schroder RR. Optimizing phase contrast in transmission electron microscopy with an electrostatic (Boersch) phase plate. *Ultramicroscopy.* 2007; 107(2–3):213–226. [PubMed: 16949755]
- Marko M, Hsieh C, Schalek R, Frank J, Mannella C. Focused-ion-beam thinning of frozen-hydrated biological specimens for cryo-electron microscopy. *Nat Methods.* 2007; 4(3):215–217. [PubMed: 17277781]
- Martin TG, Bharat TA, Joerger AC, Bai XC, Praetorius F, Fersht AR, Dietz H, Scheres SH. Design of a molecular support for cryo-EM structure determination. *Proc Natl Acad Sci U S A.* 2016; 113(47):E7456–e7463. [PubMed: 27821763]
- Matthies D, Dalmas O, Borgnia MJ, Dominik PK, Merk A, Rao P, Reddy BG, Islam S, Bartesaghi A, Perozo E, Subramaniam S. Cryo-EM Structures of the Magnesium Channel CorA Reveal Symmetry Break Upon Gating. *Cell.* 2016; 164(4):747–756. [PubMed: 26871634]
- McDowell AW, Chang JJ, Freeman R, Lepault J, Walter CA, Dubochet J. Electron microscopy of frozen hydrated sections of vitreous ice and vitrified biological samples. *J Microsc.* 1983; 131(Pt 1):1–9. [PubMed: 6350598]
- McMullan G, Chen S, Henderson R, Faruqi AR. Detective quantum efficiency of electron area detectors in electron microscopy. *Ultramicroscopy.* 2009a; 109(9):1126–1143. [PubMed: 19497671]
- McMullan G, Clark AT, Turchetta R, Faruqi AR. Enhanced imaging in low dose electron microscopy using electron counting. *Ultramicroscopy.* 2009b; 109(12):1411–1416. [PubMed: 19647366]
- McMullan G, Faruqi AR, Clare D, Henderson R. Comparison of optimal performance at 300keV of three direct electron detectors for use in low dose electron microscopy. *Ultramicroscopy.* 2014; 147:156–163. [PubMed: 25194828]
- McMullan G, Faruqi AR, Henderson R. Direct Electron Detectors. *Methods Enzymol.* 2016; 579:1–17. [PubMed: 27572721]

- McMullan G, Faruqi AR, Henderson R, Guerrini N, Turchetta R, Jacobs A, van Hoften G. Experimental observation of the improvement in MTF from backthinning a CMOS direct electron detector. *Ultramicroscopy*. 2009c; 109(9–3):1144–1147. [PubMed: 19541421]
- Merk A, Bartesaghi A, Banerjee S, Falconieri V, Rao P, Davis MI, Pragani R, Boxer MB, Earl LA, Milne JLS, Subramaniam S. Breaking Cryo-EM Resolution Barriers to Facilitate Drug Discovery. *Cell*. 2016; 165(7):1698–1707. [PubMed: 27238019]
- Meyerson JR, Rao P, Kumar J, Chittori S, Banerjee S, Pierson J, Mayer ML, Subramaniam S. Self-assembled monolayers improve protein distribution on holey carbon cryo-EM supports. *Sci Rep*. 2014; 4:7084. [PubMed: 25403871]
- Milazzo AC, Cheng A, Moeller A, Lyumkis D, Jacovetty E, Polukas J, Ellisman MH, Xuong NH, Carragher B, Potter CS. Initial evaluation of a direct detection device detector for single particle cryo-electron microscopy. *J Struct Biol*. 2011; 176(3):404–408. [PubMed: 21933715]
- Moerner WE, Orrit M. Illuminating Single Molecules in Condensed Matter. *Science*. 1999; 283(5408):1670–1676. [PubMed: 10073924]
- Murata K, Liu X, Danev R, Jakana J, Schmid MF, King J, Nagayama K, Chiu W. Zernike phase contrast cryo-electron microscopy and tomography for structure determination at nanometer and subnanometer resolutions. *Structure*. 2010; 18(8):903–912. [PubMed: 20696391]
- Murata K, Wolf M. Cryo-electron microscopy for structural analysis of dynamic biological macromolecules. *Biochim Biophys Acta, Gen Subj*. 2018; 1862(2):324–334. [PubMed: 28756276]
- Nagayama K. *Adv Imaging Electron Phys*. Elsevier; 2005. Phase Contrast Enhancement with Phase Plates in Electron Microscopy; 69–146.
- Nagayama K. Another 60 years in electron microscopy: development of phaseplate electron microscopy and biological applications. *J Electron Microsc*. 2011; 60(Suppl 1):S43–S62.
- Nagayama K, Danev R. Phase contrast electron microscopy: development of thin-film phase plates and biological applications. *Philos Trans R Soc B Biol Sci*. 2008; 363(1500):2153–2162.
- Noble AJ, Dandey VP, Wei H, Brasch J, Chase J, Acharya P, Tan YZ, Zhang Z, Kim LY, Scapin G, Rapp M, Eng ET, Rice WJ, Cheng A, Negro CJ, Shapiro L, Kwong PD, Jeruzalmi D, des Georges A, Potter CS, Carragher B. Routine Single Particle CryoEM Sample and Grid Characterization by Tomography. *bioRxiv*. 2017
- Nogales E. The development of cryo-EM into a mainstream structural biology technique. *Nat Methods*. 2015; 13:24.
- Oikonomou CM, Jensen GJ. Cellular Electron Cryotomography: Toward Structural Biology In Situ. *Ann Rev Biochem*. 2017; 86(1):873–896. [PubMed: 28426242]
- Parent KN, Tang J, Cardone G, Gilcrease EB, Janssen ME, Olson NH, Casjens SR, Baker TS. Three-dimensional reconstructions of the bacteriophage CUS-3 virion reveal a conserved coat protein I-domain but a distinct tailspike receptor-binding domain. *Virology*. 2014; 464–465:55–66.
- Parmar M, Rawson S, Scarff CA, Goldman A, Dafforn TR, Muench SP, Postis VLG. Using a SMALP platform to determine a sub-nm single particle cryo-EM membrane protein structure. *Biochim Biophys Acta*. 2018; 1860(2):378–383.
- Razinkov I, Dandey V, Wei H, Zhang Z, Melnekoff D, Rice WJ, Wigge C, Potter CS, Carragher B. A new method for vitrifying samples for cryoEM. *J Struct Biol*. 2016; 195(2):190–198. [PubMed: 27288865]
- Rhinow D, Kuhlbrandt W. Electron cryo-microscopy of biological specimens on conductive titanium-silicon metal glass films. *Ultramicroscopy*. 2008; 108(7):698705.
- Rigort A, Bauerlein FJ, Leis A, Gruska M, Hoffmann C, Laugks T, Bohm U, Eibauer M, Gnaegi H, Baumeister W, Plitzko JM. Micromachining tools and correlative approaches for cellular cryo-electron tomography. *J Struct Biol*. 2010; 172(2):169–179. [PubMed: 20178848]
- Rigort A, Villa E, Bäuerlein FJB, Engel BD, Plitzko JM. Chapter 14 - Integrative Approaches for Cellular Cryo-electron Tomography: Correlative Imaging and Focused Ion Beam Micromachining. In: Müller-Reichert T, Verkade P, editors *Methods Cell Biol*. Academic Press; 2012. 259–281.
- Rohou A, Grigorieff N. CTFFIND4: Fast and accurate defocus estimation from electron micrographs. *J Struct Biol*. 2015; 192(2):216–221. [PubMed: 26278980]

- Russo CJ, Passmore LA. Controlling protein adsorption on graphene for cryo-EM using low-energy hydrogen plasmas. *Nat Methods*. 2014a; 11(6):649–652. [PubMed: 24747813]
- Russo CJ, Passmore LA. Electron microscopy: Ultrastable gold substrates for electron cryomicroscopy. *Science*. 2014b; 346(6215):1377–1380. [PubMed: 25504723]
- Russo CJ, Passmore LA. Progress towards an optimal specimen support for electron cryomicroscopy. *Curr Opin Struct Biol*. 2016a; 37:81–89. [PubMed: 26774849]
- Russo CJ, Passmore LA. Ultrastable gold substrates: Properties of a support for high-resolution electron cryomicroscopy of biological specimens. *J Struct Biol*. 2016b; 193(1):33–44. [PubMed: 26592474]
- Sander B, Golas MM, Stark H. Advantages of CCD detectors for de novo three-dimensional structure determination in single-particle electron microscopy. *J Struct Biol*. 2005; 151(1):92–105. [PubMed: 15946861]
- Sartori A, Gatz R, Beck F, Rigort A, Baumeister W, Plitzko JM. Correlative microscopy: bridging the gap between fluorescence light microscopy and cryo-electron tomography. *J Struct Biol*. 2007; 160(2):135–145. [PubMed: 17884579]
- Schellenberger P, Kaufmann R, Siebert CA, Hagen C, Wodrich H, Grünwald K. High-precision correlative fluorescence and electron cryo microscopy using two independent alignment markers. *Ultramicroscopy*. 2014; 143:41–51. [PubMed: 24262358]
- Schmidt C, Urlaub H. Combining cryo-electron microscopy (cryo-EM) and cross-linking mass spectrometry (CX-MS) for structural elucidation of large protein assemblies. *Curr Opin Struct Biol*. 2017; 46:157–168. [PubMed: 29080436]
- Schorb M, Briggs JA. Correlated cryo-fluorescence and cryo-electron microscopy with high spatial precision and improved sensitivity. *Ultramicroscopy*. 2014; 143:24–32. [PubMed: 24275379]
- Schorb M, Gaechter L, Avinoam O, Sieckmann F, Clarke M, Bebeacua C, Bykov YS, Sonnen AFP, Lihl R, Briggs JAG. New hardware and workflows for semi-automated correlative cryo-fluorescence and cryo-electron microscopy/tomography. *J Struct Biol*. 2017; 197(2):83–93. [PubMed: 27368127]
- Schroder RR. Zero-loss energy-filtered imaging of frozen-hydrated proteins: model calculations and implications for future developments. *J Microsc*. 1992; 166(Pt 3):389–400. [PubMed: 1495093]
- Schroder RR. Advances in electron microscopy: A qualitative view of instrumentation development for macromolecular imaging and tomography. *Arch Biochem Biophys*. 2015; 581:25–38. [PubMed: 26032338]
- Schultheiss K, Zach J, Gamm B, Dries M, Frindt N, Schröder RR, Gerthsen D. New Electrostatic Phase Plate for Phase-Contrast Transmission Electron Microscopy and Its Application for Wave-Function Reconstruction. *Microsc Microanal*. 2010; 16(6):785–794. [PubMed: 20946700]
- Schwartz CL, Sarbash VI, Ataullakhanov FI, McIntosh JR, Nicastro D. Cryo-fluorescence microscopy facilitates correlations between light and cryo-electron microscopy and reduces the rate of photobleaching. *J Microsc*. 2007; 227(2):98–109. [PubMed: 17845705]
- Shaikh TR, Yassin AS, Lu Z, Barnard D, Meng X, Lu TM, Wagenknecht T, Agrawal RK. Initial bridges between two ribosomal subunits are formed within 9.4 milliseconds, as studied by time-resolved cryo-EM. *Proc Natl Acad Sci U S A*. 2014; 111(27):9822–9827. [PubMed: 24958863]
- Sharp TH, Koster AJ, Gros P. Heterogeneous MAC Initiator and Pore Structures in a Lipid Bilayer by Phase-Plate Cryo-electron Tomography. *Cell Rep*. 2016; 15(1):1–8. [PubMed: 27052168]
- Shen PS, Yang X, DeCaen PG, Liu X, Bulkley D, Clapham DE, Cao E. The Structure of the Polycystic Kidney Disease Channel PKD2 in Lipid Nanodiscs. *Cell*. 2016; 167(3):763–773.e711. [PubMed: 27768895]
- Stagg SM, Lander GC, Pulokas J, Fellmann D, Cheng A, Quispe JD, Mallick SP, Avila RM, Carragher B, Potter CS. Automated cryoEM data acquisition and analysis of 284742 particles of GroEL. *J Struct Biol*. 2006; 155(3):470–481. [PubMed: 16762565]
- Stark H. GraFix: stabilization of fragile macromolecular complexes for single particle cryo-EM. *Methods Enzymol*. 2010; 481:109–126. [PubMed: 20887855]
- Strauss JD, Hammonds JE, Yi H, Ding L, Spearman P, Wright ER. Three-dimensional structural characterization of HIV-1 tethered to human cells. *J Virol*. 2016; 90(3):1507–1521. [PubMed: 26582000]

- Studer D, Humbel BM, Chiquet M. Electron microscopy of high pressure frozen samples: bridging the gap between cellular ultrastructure and atomic resolution. *Histochem Cell Biol.* 2008; 130(5): 877–889. [PubMed: 18795316]
- Subramaniam S, Kuhlbrandt W, Henderson R. CryoEM at IUCrJ: a new era. *IUCrJ.* 2016; 3(Pt 1):3–7.
- Sun C, Benlekbir S, Venkatakrishnan P, Wang Y, Hong S, Hosler J, Tajkhorshid E, Rubinstein JL, Gennis RB. Structure of the alternative complex III in a supercomplex with cytochrome oxidase. *Nature.* 2018
- Tan YZ, Baldwin PR, Davis JH, Williamson JR, Potter CS, Carragher B, Lyumkis D. Addressing preferred specimen orientation in single-particle cryo-EM through tilting. *Nat Methods.* 2017; 14(8):793–796. [PubMed: 28671674]
- Tanner JR, D AC, Dukes MJ, Melanson LA, McDonald SM, Kelly DF. Cryo-SiN - an alternative substrate to visualize active viral assemblies. *J Analyt Molecul Tech.* 2013; 1(1):6.
- Taylor KA, Glaeser RM. Electron diffraction of frozen, hydrated protein crystals. *Science.* 1974; 186(4168):1036–1037. [PubMed: 4469695]
- Thompson RF, Walker M, Siebert CA, Muench SP, Ranson NA. An introduction to sample preparation and imaging by cryo-electron microscopy for structural biology. *Methods.* 2016; 100:3–15. [PubMed: 26931652]
- Unwin N. Acetylcholine receptor channel imaged in the open state. *Nature.* 1995; 373(6509):37–43. [PubMed: 7800037]
- Unwin N, Fujiyoshi Y. Gating movement of acetylcholine receptor caught by plunge-freezing. *J Mol Biol.* 2012; 422(5):617–634. [PubMed: 22841691]
- van Driel LF, Valentijn JA, Valentijn KM, Koning RI, Koster AJ. Tools for correlative cryo-fluorescence microscopy and cryo-electron tomography applied to whole mitochondria in human endothelial cells. *Eur J Cell Biol.* 2009; 88(11):669–684. [PubMed: 19726102]
- von der Ecken J, Muller M, Lehman W, Manstein DJ, Penczek PA, Raunser S. Structure of the F-actin-tropomyosin complex. *Nature.* 2015; 519(7541):114–117. [PubMed: 25470062]
- von Loeffelholz O, Papai G, Danev R, Myasnikov AG, Natchiar SK, Hazemann I, Menetret JF, Klaholz BP. Volta phase plate data collection facilitates image processing and cryo-EM structure determination. *J Struct Biol.* 2018
- Voorhees RM, Fernandez IS, Scheres SH, Hegde RS. Structure of the mammalian ribosome-Sec61 complex to 3.4 Å resolution. *Cell.* 2014; 157(7):1632–1643. [PubMed: 24930395]
- Walker M, Trinick J, White H. Millisecond time resolution electron cryo-microscopy of the M-ATP transient kinetic state of the acto-myosin ATPase. *Biophys J.* 1995; 68(4 Suppl):87S–91S. [PubMed: 7787114]
- Walker M, Zhang X-Z, Jiang W, Trinick J, White HD. Observation of transient disorder during myosin subfragment-1 binding to actin by stopped-flow fluorescence and millisecond time resolution electron cryomicroscopy: Evidence that the start of the crossbridge power stroke in muscle has variable geometry. *Proc Natl Acad Sci U S A.* 1999; 96(2):465–470. [PubMed: 9892656]
- Walter A, Muzik H, Vieker H, Turchanin A, Beyer A, Golzhauser A, Lacher M, Steltenkamp S, Schmitz S, Holik P, Kuhlbrandt W, Rhinow D. Practical aspects of Boersch phase contrast electron microscopy of biological specimens. *Ultramicroscopy.* 2012; 116:62–72. [PubMed: 22537744]
- Wan RX, Yan CY, Bai R, Wang L, Huang M, Wong CCL, Shi YG. The 3.8 Å structure of the U4/U6.U5 tri-snRNP: Insights into spliceosome assembly and catalysis. *Science.* 2016; 351(6272):466–475. [PubMed: 26743623]
- Wan W, Briggs JAG. Chapter Thirteen - Cryo-Electron Tomography and Subtomogram Averaging. In: Crowther RA, editor *Methods Enzymol.* Academic Press; 2016. 329367
- Wang L, Ounjai P, Sigworth FJ. Streptavidin crystals as nanostructured supports and image-calibration references for cryo-EM data collection. *J Struct Biol.* 2008; 164(2):190–198. [PubMed: 18707004]
- Wei H, Dandey VP, Zhang Z, Raczkowski A, Rice WJ, Carragher B, Potter CS. Optimizing “Self-Wicking” Nanowire Grids. *J Struct Biol.* 2018
- Wilkes M, Madej MG, Kreuter L, Rhinow D, Heinz V, De Sanctis S, Ruppel S, Richter RM, Joos F, Grieben M, Pike ACW, Huiskonen JT, Carpenter EP, Kühlbrandt W, Witzgall R, Ziegler C.

- Molecular insights into lipid-assisted Ca<sup>2+</sup> regulation of the TRP channel Polycystin-2. *Nat Struct Mol Biol.* 2017; 24:123. [PubMed: 28092368]
- Wolf SG, Mutsafi Y, Horowitz B, Elbaum M, Fass D. Cryo-Stem Tomography Provides Morphological and Chemical Characterization of Precipitated Calcium-Phosphate Clusters Sequestered in Mitochondria of Intact Vitrified Fibroblasts. *Biophys J.* 2016; 110(3):23a.
- Yoshioka C, Carragher B, Potter CS. Cryomesh: a new substrate for cryo-electron microscopy. *Microsc Microanal.* 2010; 16(1):43–53. [PubMed: 20082728]
- Yu G, Li K, Huang P, Jiang X, Jiang W. Antibody-Based Affinity Cryoelectron Microscopy at 2.6-Å Resolution. *Structure.* 2016a; 24(11):1984–1990. [PubMed: 27806259]
- Yu G, Li K, Jiang W. Antibody-based affinity cryo-EM grid. *Methods.* 2016b; 100:16–24. [PubMed: 26804563]
- Yu G, Vago F, Zhang D, Snyder JE, Yan R, Zhang C, Benjamin C, Jiang X, Kuhn RJ, Serwer P, Thompson DH, Jiang W. Single-step antibody-based affinity cryo-electron microscopy for imaging and structural analysis of macromolecular assemblies. *J Struct Biol.* 2014; 187(1):1–9. [PubMed: 24780590]
- Zhang J, Ma B, DiMaio F, Douglas NR, Joachimiak LA, Baker D, Frydman J, Levitt M, Chiu W. Cryo-EM Structure of a Group II Chaperonin in the Prehydrolysis ATP-Bound State Leading to Lid Closure. *Structure.* 2011; 19(5):633–639. [PubMed: 21565698]
- Zhang P. Correlative Cryo-electron Tomography and Optical Microscopy of Cells. *Curr Opin Struct Biol.* 2013; 23(5)doi: 10.1016/j.sbi.2013.1007.1017

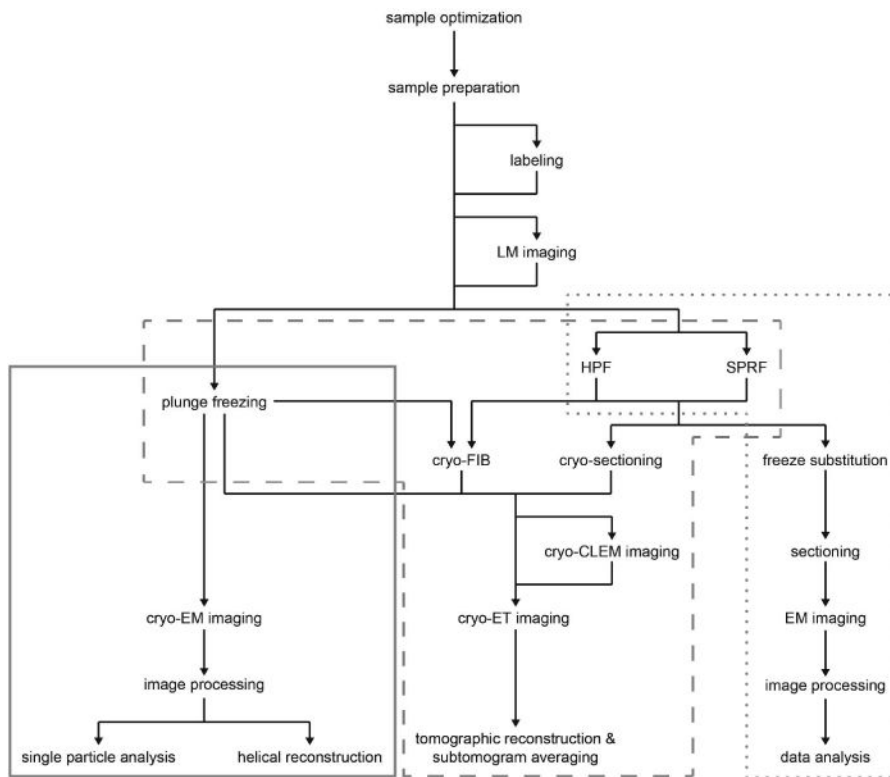


**Figure 1. Cryo-EM workflow**

Schematic illustration of options for cryo-EM sample preparation, imaging, and data processing. Solid gray box indicates methods typically used for single particle analysis; dashed gray box indicates methods typically used for cryo-ET; dotted gray box indicates methods typically used for conventional EM sectioning. LM, light microscopy; HPF, high pressure freezing; SPRF, self-pressurized rapid freezing; FIB, focused ion beam; CLEM, correlated light and electron microscopy; EM, electron microscopy.



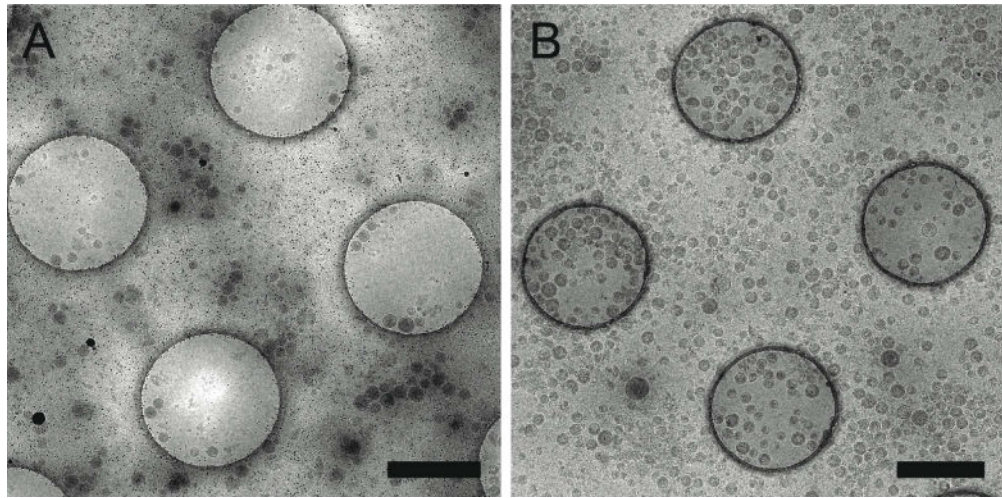


**Figure 2. Affinity grid designed to selectively capture virus-like particles (VLPs)**  
Cryo-EM images of HIV CD84 VLPs applied to an untreated grid (**A**) and a 20% Ni-NTA cryo-affinity grid with His-tagged Protein A and anti-Env polyclonal antibody (**B**). Use of the affinity capture method leads to increased VLP concentration and improved particle distribution on the grid. See Kiss *et al.* (Kiss, et al., 2014) for experimental detail. Scale bars, 1  $\mu\text{m}$ .

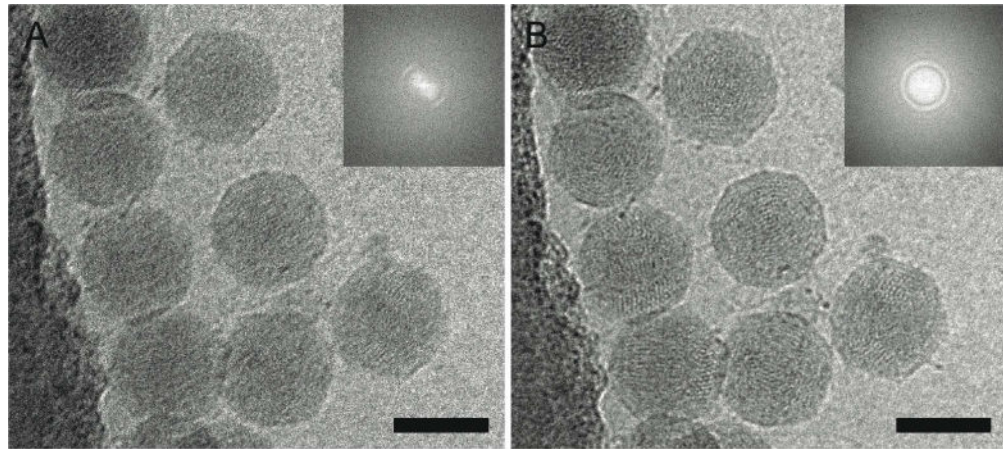


**Figure 3. Motion correction of data recorded on a Direct Electron DE-20 direct electron detection device significantly improves image quality**

2D projection cryo-EM image of coliphage BA14 particles before (**A**) and after (**B**) motion correction using Direct Electron, LP scripts and the corresponding power spectra (insets).

The image was recorded at a frame rate of 12 frames per second with an exposure time of 5 seconds. Scale bars, 50 nm.

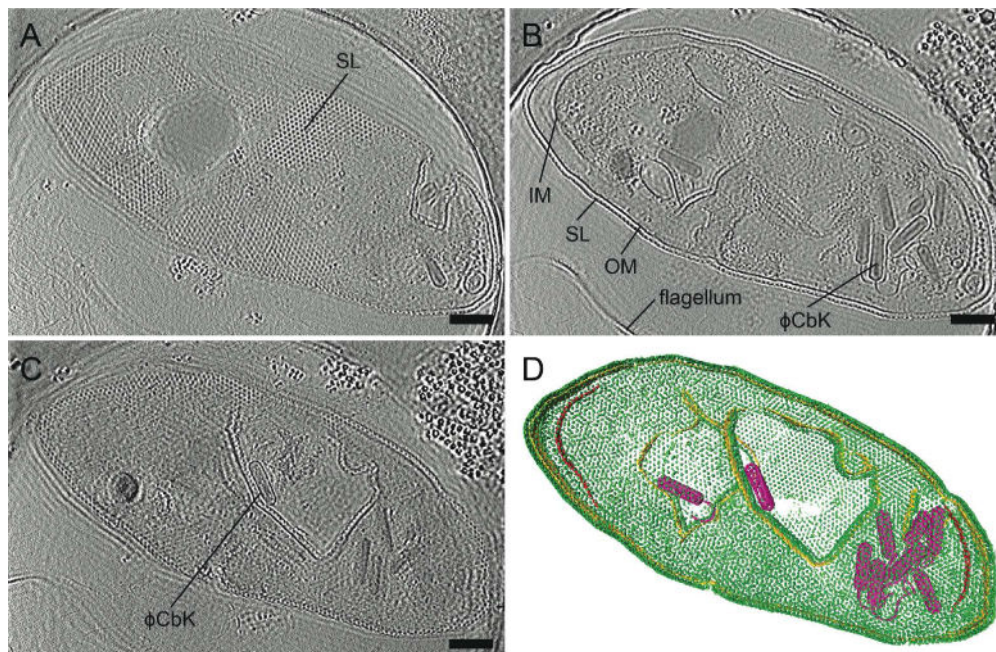


**Figure 4. Zernike phase plate imaging of a phage-lysed bacterial cell provides contrast, revealing internal features**

Cryo-ET slices of  $\phi$ CbK phage-lysed *Caulobacter crescentus* cell using ZPC at zero defocus. (A) A top slice of the tomogram illustrating the hexagonal surface layer (SL), (B) a central slice revealing newly assembled phages within the lysing cell, and (C) a central slice showing an assembled phage capsid in the process of genome packaging. Fringing artifacts are evident, particularly at the edge of the cell. (D) Corresponding 3D segmentation showing surface layer, SL, green; outer membrane, OM, gold; inner membrane, IM, red; and  $\phi$ CbK, magenta. Scale bars, 200 nm.

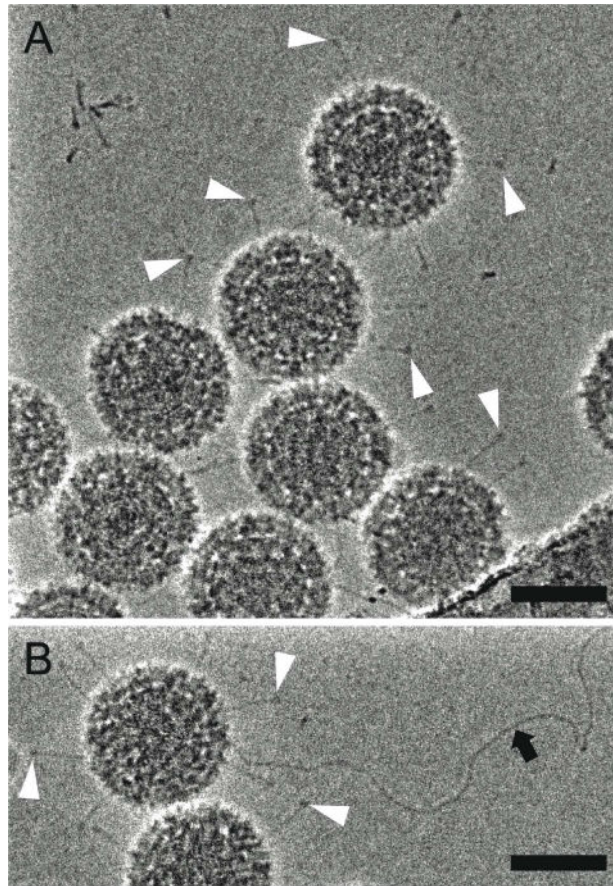


**Figure 5. Hole-free phase plate (HFPP) imaging provides enhanced contrast without strong fringing artifacts**

Cryo-EM images of reovirus T1L particles using HFPP slightly underfocus. (**A and B**) reovirus T1L particles displaying attachment fibers as indicated by white arrowheads. The black arrow points to a released viral genome in (**B**). Scale bars, 50 nm.

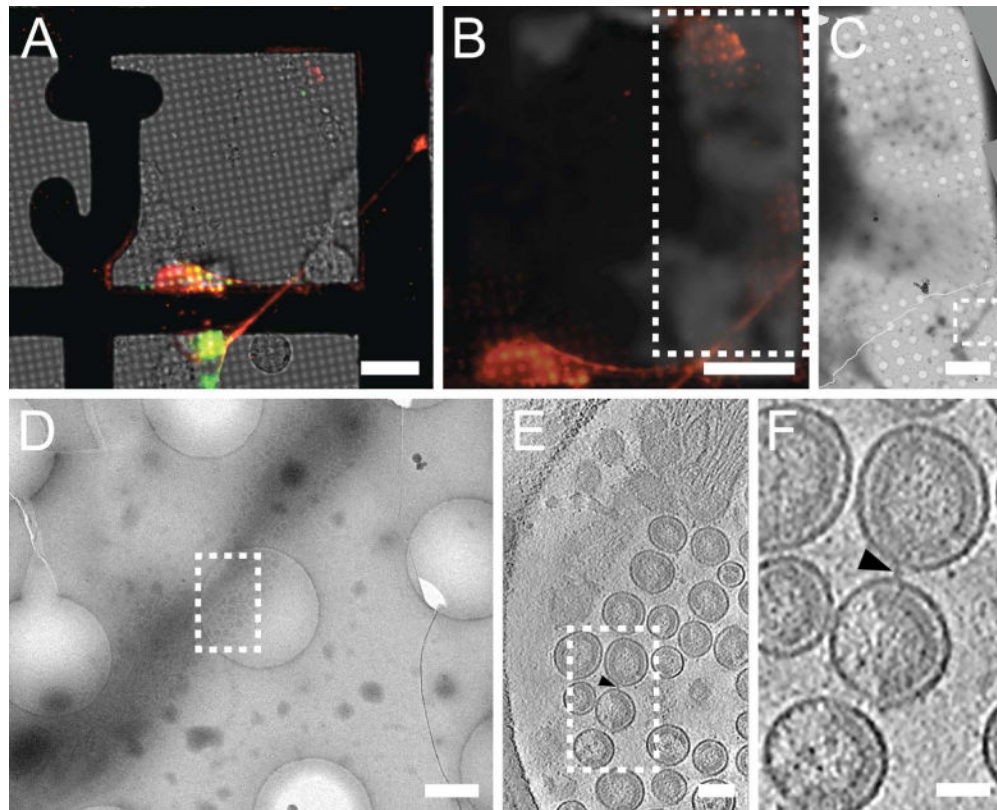


**Figure 6. CLEM imaging of transfected mammalian cells provides multi-scale information**  
 HT1080 cells grown on a gold London Finder grid and transfected with EGFP-tetherin (green) and mCherry-Gag (red) were imaged by live cell fluorescence microscopy (**A** and **B**), then plunge frozen and imaged by cryo-EM montage (**C** and **D**), and cryo-ET (**E** and **F**). The mCherry-Gag (red) signal in (**A**) and (**B**) corresponds to electron density of a thin cellular extension in (**C**) and (**D**). The black arrowheads in (**E**) and (**F**) indicate a tether attaching 2 VLPs. Dashed boxes correspond to the enlarged image in the next panel. Adapted from Strauss *et al.* (Strauss, et al., 2016). Scale bars, (**A** and **B**) 25  $\mu\text{m}$ , (**C**) 10  $\mu\text{m}$ , (**D**) 500 nm, (**E**) 100 nm, and (**F**) 50 nm.

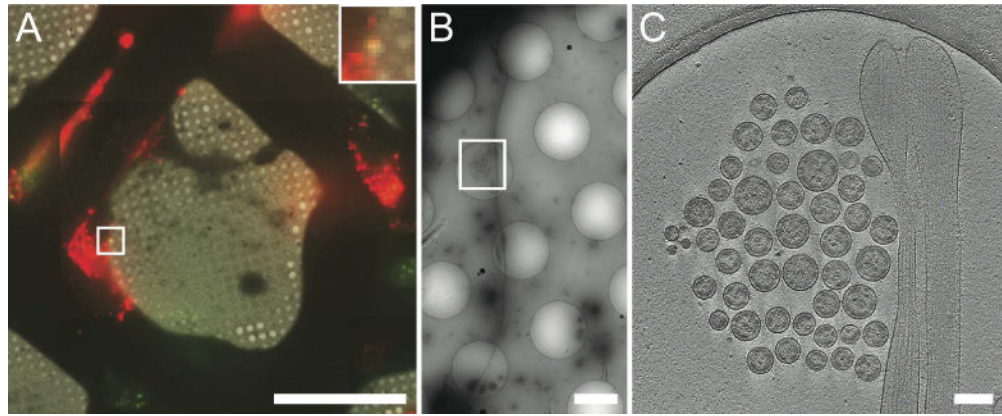


**Figure 7. Cryo-CLEM imaging of transfected mammalian cells**

HT1080 cells transfected with EGFP-tetherin (green) and mCherry-Gag (red) imaged by cryo-fluorescence microscopy (**A**), cryo-EM montaging (**B**), and cryo-ET (**C**). Dashed boxes correspond to the enlarged image in the next panel. The yellow signal in (**A**) (inset) indicates colocalization of EGFP-tetherin (green) and mCherry-Gag (red) signal and corresponds to a cluster of HIV-1 VLPs tethered to a cellular extension in (**B**) and (**C**). Adapted from Hampton *et al.* (Hampton, et al., 2017). Scale bars, (**A**) 50  $\mu\text{m}$ , inset is 3X, (**B**) 2  $\mu\text{m}$ , (**C**) 200 nm.